





**INVESTIGATION OF  
AGRICULTURAL DAMAGES CAUSED BY AIR POLLUTION OVER EUROPE  
BY USING WRF/CMAQ MODELLING SYSTEM**

**M.Sc. THESIS**

**Yaşar Burak ÖZTANER**

**Climate and Marine Sciences**

**Earth System Sciences**

**MAY 2016**





**INVESTIGATION OF  
AGRICULTURAL DAMAGES CAUSED BY AIR POLLUTION OVER EUROPE  
BY USING WRF/CMAQ MODELLING SYSTEM**

**M.Sc. THESIS**

**Yaşar Burak ÖZTANER  
(601131005)**

**Climate and Marine Sciences**

**Earth System Sciences**

**Thesis Advisor: Prof. Dr. Alper ÜNAL**

**MAY 2016**



**WRF/CMAQ MODELLEME SİSTEMİ İLE  
HAVA KİRLİLİĞİNDEN KAYNAKLANAN  
AVRUPA'DAKİ TARIMSAL ZARARIN İNCELENMESİ**

**YÜKSEK LİSANS TEZİ**

**Yaşar Burak ÖZTANER  
(601131005)**

**İklim ve Deniz Bilimleri**

**Yer Sistem Bilimleri**

**Tez Danışmanı: Prof. Dr. Alper ÜNAL**

**MAYIS 2016**



Yaşar Burak ÖZTANER, a M.Sc. student of ITU Eurasia Institute of Earth Sciences 601131005 successfully defended the thesis entitled “INVESTIGATION OF AGRICULTURAL DAMAGES CAUSED BY AIR POLLUTION OVER EUROPE BY USING WRF/CMAQ MODELLING SYSTEM”, which he prepared after fulfilling the requirements specified in the associated legislations, before the jury whose signatures are below.

**Thesis Advisor :**     **Prof. Dr. Alper ÜNAL** .....  
Istanbul Technical University

**Jury Members :**     **Assist. Prof. Dr. Burçak KAYNAK TEZEL** .....  
Istanbul Technical University

**Prof. Dr. Mete TAYANÇ** .....  
Marmara University

**Date of Submission :**    **02 May 2016**

**Date of Defense :**        **07 June 2016**



*To all my family,*





## FOREWORD

I would like to express my sincere gratitude and thanks to several people for having helped me during my M.Sc. First, I would like to express my deepest appreciation to my advisor Prof. Dr. Alper Ünal for his understanding, support, guidance, and encouragement throughout my study and providing me the trust. I would like to thank him for giving me numerous opportunities during my M.Sc. degree.

Secondly, I would like to express my very special thanks to Dr. Luca Pozzoli from JRC-European Commission's Science Service (Italy) and Associate Prof. Dr. Amir Hakami from Carleton University (Canada) for their support in this study, encouragements and sharing valuable experience in air quality modeling field. I am also very grateful to Prof Dr. Özgür Kayalica from Istanbul Technical University, Department of Management Engineering for his help and valuable guidance in the interpretation of economic values. Also I am grateful to Prof. Dr. Tayfun Kindap from Istanbul Technical University, Eurasia Institute of Earth Science (Turkey) and Dt. Güngör Doğaner. I am grateful to Dr. Yasemin Ergüner for her endless trust and discussions she provided during my M.Sc. degree. I will always gratefully remember their support in times when I felt depressed and like giving up.

Very special thanks to M.Sc. Metin Baykara for his valuable contribution in my thesis revising the manuscript and guidance of the study. I wish him success in his PhD. Also, I am grateful to Giuseppe Baldassare for his assistance in fire emissions part of the study. I would like to thank my colleagues, Burcu Kabataş, Duygu Özçomak, Elvin Öksüz, Merve Gökgöz Ergül, Müge Kafadar, Seden Baltacıbaşı. Not only are they colleagues of mine, but also my closest friends. I would also like to thank them as good friends and wish them success in their life.

Special thanks to Pertevniyal 1872, as a member of the team and D'Team, Barış Dolan, Emre Karabulut, Emre Çubuklu, Onur Çevik for their understanding and encouragement during my M.Sc. studies. They are not just only my friends; they are also like a family.

Finally and most importantly, I would like to express my sincere thanks to my most beloved family, my brother Burhan Öztaner, my mother Ferzan Öztaner and my father Metin Öztaner for their continuous support on this work and encouraging me on my career.

May 2016

Yaşar Burak ÖZTANER



## TABLE OF CONTENTS

	<u>Page</u>
<b>FOREWORD.....</b>	<b>ix</b>
<b>TABLE OF CONTENTS.....</b>	<b>xi</b>
<b>ABBREVIATIONS .....</b>	<b>xiii</b>
<b>SYMBOLS .....</b>	<b>xv</b>
<b>LIST OF TABLES .....</b>	<b>xvii</b>
<b>LIST OF FIGURES .....</b>	<b>xix</b>
<b>SUMMARY .....</b>	<b>xxi</b>
<b>ÖZET .....</b>	<b>xxv</b>
<b>1. INTRODUCTION .....</b>	<b>1</b>
1.1 Objective.....	7
<b>2. DATA &amp; METHODOLOGY .....</b>	<b>9</b>
2.1 Ozone Observations and Study Period .....	9
2.2 Distribution of the Wheat Production.....	10
2.3 Modeling Framework .....	13
2.3.1 Meteorological Modeling .....	14
2.3.1.1 Weather Research and Forecast Model (WRF) .....	14
2.3.1.2 WRF-ARW Programs.....	15
geogrid Module .....	15
ungrib Module .....	16
metgrid Module .....	17
real Module .....	17
wrf Module.....	18
2.3.1.3 WRF-ARW Setup .....	18
2.3.2 Emission Processing.....	19
2.3.2.1 Anthropogenic Emissions.....	20
2.3.2.2 Biogenic Emissions .....	21
2.3.2.3 Wildfire Emissions.....	21
2.3.3 Chemical Transport Model .....	23
2.3.3.1 The Community Multi-Scale Air Quality Model (CMAQ).....	23
2.3.3.2 Major Modules of CMAQ .....	24
Photolysis Rate Preprocessor (JPROC).....	24
Initial Conditions Processor (ICON).....	25
Boundary Conditions Processor (BCON) .....	25
Meteorology-Chemistry Interface Processor (MCIP) .....	25
CMAQ Chemistry-Transport Model (CCTM) .....	26
2.3.3.3 Input Data and Chemical Mechanism.....	26

2.3.4 Calculation of the Crop Production Loss and Economic Damages .....	27
<b>3. RESULTS &amp; DISCUSSION.....</b>	<b>31</b>
3.1 Model Performance .....	31
3.2 Crop Production Loss .....	32
3.3 Economic Damages .....	39
<b>4. CONCLUSION .....</b>	<b>45</b>
<b>REFERENCES.....</b>	<b>49</b>
<b>APPENDICES .....</b>	<b>55</b>
APPENDIX A .....	57
APPENDIX B.....	59
APPENDIX C.....	61
APPENDIX D .....	63
<b>CURRICULUM VITAE .....</b>	<b>67</b>

## ABBREVIATIONS

<b>AOT40</b>	: Accumulated Exposure over a threshold of 40 ppb index
<b>BCON</b>	: Boundary Condition Processor
<b>CCTM</b>	: Biogenic Volatile Organic Compounds
<b>CMAQ</b>	: Community Multiscale Air Quality
<b>CONUS</b>	: Continental United States
<b>CP</b>	: Crop Production
<b>CPL</b>	: Crop Production Loss
<b>CR</b>	: Crop-Response Function
<b>ECMWF</b>	: European Centre for Medium-Range Weather Forecasting
<b>EEA</b>	: European Environmental Agency
<b>EL</b>	: Economic Loss
<b>FAO</b>	: Food and Agriculture Organization
<b>UN</b>	: United Nations
<b>GDP</b>	: Gross Domestic Product
<b>GFAS</b>	: Global Fire Assimilation System
<b>HTAP</b>	: The Task Force on Hemispheric Transport of Air Pollution
<b>ICON</b>	: Initial Condition Processor
<b>JPROC</b>	: Photolysis Rate Processor
<b>M7</b>	: Mean of 7 hours Index
<b>MACC</b>	: Monitoring and Atmospheric Composition and Climate
<b>MCIP</b>	: Meteorology-Chemistry Interface Processor
<b>MM5</b>	: Fifth-Generation Penn State/NCAR Mesoscale Model
<b>MODIS</b>	: Moderate Resolution Imaging Spectroradiometer
<b>NCAR</b>	: National Center for Atmospheric Research
<b>NCEP</b>	: National Centers for Environmental Prediction
<b>NOAA</b>	: National Oceanic and Atmospheric Administration
<b>NO<sub>x</sub></b>	: Nitrogen oxides
<b>RY</b>	: Relative Yield
<b>RYL</b>	: Relative Yield Loss
<b>SEVIRI</b>	: Spinning Enhanced Visible and Infrared Imager
<b>SNAP</b>	: Selection of Nomenclature for Air Pollutants Prototype
<b>TNO</b>	: Netherlands Organization for Applied Scientific Research
<b>WRF</b>	: Weather Research & Forecasting Model
<b>USEPA</b>	: Environmental Protection Agency, USA
<b>EU</b>	: European Union
<b>UK</b>	: United Kingdom
<b>VOCs</b>	: Volatile Organic Compounds



## SYMBOLS

$\text{‰}$	:	Parts per Thousand
\$	:	United State's Dollar Currency
%	:	percent
Mt	:	Million metric Ton
$\mu m$	:	Micrometer
M	:	Million
bn	:	Billion
<i>ppm</i>	:	Parts per million
<i>ppb</i>	:	Parts per billion
$\text{W/m}^2$	:	Watt per square meter
$^{\circ}$	:	Degree





## LIST OF TABLES

	<u>Page</u>
<b>Table 2.1</b> : Description of ozone exposure indices.....	27
<b>Table 2.2</b> : Crop Exposure- Response (CR) functions for wheat used in the study to assess the Relative Yield Losses (RYL) .....	28
<b>Table 3.1</b> : Regional calculated total economic loss (\$ Billion).....	40
<b>Table A.1</b> : Model Performance Analysis for Temperature at 2m for Each Station at the nested domain (10km resl.).....	57
<b>Table B.1</b> : Country-Specific Total Wheat Production and Total Crop Production Loss for three Ozone Exposure Indices .....	59
<b>Table B.2</b> : Country-Specific Percentage of Total Crop Production Loss for three Ozone Exposure Indices .....	60
<b>Table C.1</b> : Country-Specific FAO 2009 Producer Price [USD] and Total Economic Loss [USD] for three Ozone Exposure Indices .....	61
<b>Table C.2</b> : Country-Specific Economic Damages in terms of EL/GDP (percentage) (normalized values to make comparison) .....	62



## LIST OF FIGURES

	<u>Page</u>
<b>Figure 1.1</b> : Average Monthly Surface Ozone at Zugspitze station, Germany .....	3
<b>Figure 1.2</b> : Time series of seasonal mean O <sub>3</sub> concentrations at three European mountain locations, Jungfraujoch, Zugspitz and Sonnblick .....	3
<b>Figure 1.3</b> : Ozone injury on (a) white clover, (b) brown knapweed and (c) violet	4
<b>Figure 1.4</b> : The more wheat is exposed to ozone pollution, the more its growth is reduced .....	5
<b>Figure 1.5</b> : The Relationship between Ozone and Relative Yield for six agricultural products .....	5
<b>Figure 1.6</b> : Country Specific Total Wheat Production for the year of 2009 over continental Europe .....	8
<b>Figure 2.1</b> : Mean Ozone Concentrations During Growing Season of the year 2009 over the Europe .....	10
<b>Figure 2.2</b> : Diurnal Cycle of Ozone in growing season of 2009 (May-July) and annual average of 2009 .....	10
<b>Figure 2.3</b> : Global Wheat Production (ton) for the year 2000 .....	11
<b>Figure 2.4</b> : Global Wheat Yield per hectare for the year 2000 .....	12
<b>Figure 2.5</b> : Wheat Production for the year of 2009 (FAO based-30 km x 30 km)	12
<b>Figure 2.6</b> : Flow Chart of Methodology in the Study .....	13
<b>Figure 2.7</b> : WRF Modeling System Flow chart .....	15
<b>Figure 2.8</b> : WRF Modeling Domain - 30 km x 30 km spatial resolution .....	19
<b>Figure 2.9</b> : CMAQ Model Framework .....	24
<b>Figure 3.1</b> : CMAQ Model Performance- Mean Normalized Bias Results for Each Station in the AirBase .....	32
<b>Figure 3.2</b> : Station based and model based CPL results for AOT40 metric (a,b), W126 (c,d) and M7 (e,f) .....	35
<b>Figure 3.3</b> : Total production loss in the each country for AOT40 (a), W126 (b) and M7 (c) .....	37
<b>Figure 3.4</b> : Total percentage (fractional) loss in the each country for AOT40 (a), W126 (b) and M7 (c) .....	38
<b>Figure 3.5</b> : Total Economic loss in the each country studied for AOT40 (a), W126 (b) and M7 (c) .....	41
<b>Figure 3.6</b> : Economic loss GDP in the each country studied for AOT40 (a), W126 (b) and M7 (c) .....	42
<b>Figure A.1</b> : Modelled (line) and Observed (dash-line) 2-m Temperature (°C ) Time Series for 9 stations: (a) Antalya, (b) Aydın, (c) Diyarbakır, (d) Erzurum, (e) İnebolu, (f) Kırklareli, (g) Konya, (h) Muğla, (i) Trabzon .....	58

**Figure D.1 :** Mean Normalized Error (MNE) Results (%) for Each Station in  
the Airbase ..... 63

**Figure D.2 :** Root Mean Square Error (RMSE) Results (ppb) for Each Station  
in the Airbase ..... 64

# **INVESTIGATION OF AGRICULTURAL DAMAGES CAUSED BY AIR POLLUTION OVER EUROPE BY USING WRF/CMAQ MODELLING SYSTEM**

## **SUMMARY**

The population of Europe, including non-EU countries located in continental Europe, is estimated to be around 740 million, which corresponds to 10% of the world's population (United Nations-UN, 2015). Wheat production in between 1996-2014 in Europe is 133.9 million tons (Mt). This corresponds to 21% of world's wheat production (FAO, 2015). In addition, because of Industrial Revolution in Europe an increasing trend in air pollution and pollutants that persists up to present day can be observed. This increase in air pollution is the cause of critical environmental impacts. Even though there are various studies in Europe about impacts of ozone on human health, not many studies exist to investigate ozone's impact on agriculture. Besides the negative impact on human health, exposure to high concentrations of ozone is a threat to food security and agricultural activities.

Elevated O<sub>3</sub> concentrations and changes in the concentrations affect plant life functions such as photosynthesis, transpiration, and gas exchanges. It has been found by many scientific studies that ground-level ozone exposure reduces photosynthesis of crops since it damages substomatal apoplast, cell membranes and walls. Decreased photosynthesis result in low growth rates in terms of volume or biomass. In Europe and United States of America (USA), various observational and experimental studies conducted on this subject. These studies resulted in different empirical ozone exposure equations for different parts of the world. Agricultural production losses can be calculated because of these equations. In Europe, AOT40 (cumulative summation of differences in high ozone concentrations over 40 ppb) is a widely used method which is a product of experimental studies conducted in Europe. However, in USA, W126 method (summation of weighted ozone concentrations in day light time by using sigmoidal distribution equation) is being widely used. Other than these two methods there are many other methods used around the world to calculate agricultural production loss due to ozone impacts. Some of these methods are daily summation of difference of threshold values (SUM-X method) or daily mean calculation (M-X method).

There are several studies from different parts of the world that were conducted on the impacts of ozone on agricultural crops (i.e., wheat, soybean, rice, potato), their yield losses, and relative yield losses. In a study by USEPA, a 10% crop loss due to ozone was observed in agricultural production in USA. A similar study for the Europe found that the loss was around 5% in Europe. Tropospheric ozone as a regional and global threat to plants threatens our current and future food security.

In literature, there are studies conducted on impacts of ozone on agricultural productions for different regions in the world. Even though these studies can show

the local loss, they fail to perform well for regional impacts. For this reason, some scientific studies focused on quantifying the impact of ozone pollution on crops using regional or global atmospheric models. Low spatial resolution of global models affects the level of representation of results. Spatial resolution is better in regional studies compared to global ones, however, there are studies utilizing this higher resolution to calculate agricultural production losses. In a study, in India, conducted on impacts of ozone on wheat production loss using WRF/Chem regional chemical transportation model it was found that wheat production loss was 5 Mt for 2005. In a similar study, Eta-CMAQ regional chemical transport model was used to estimate the soybean loss in USA (2005), and found that amount of loss was in range of 1.7-14.2 %. Due to regional changes in ozone concentrations, working with a regional chemistry model yields better results for the calculation of agricultural production loss. In global models, there are many uncertainties due to low resolutions.

In this study, WRF/CMAQ modeling system with three different ozone crop exposure indices (AOT40, W126, and M7) was used to estimate wheat production loss in Europe. Growing season was selected as May – July for wheat in Europe. European Environmental Agency (EEA) AirBase database ozone observations were used to calculate mean ozone values for growing season of years 2008 to 2012. The highest growing season average (45.6 ppb) was found in 2009. Averages for other years are as follows, 33.28 ppb for 2008, 29.29 ppb for 2010, 39.12 ppb for 2011, and 30.42 for 2012. This is the reason behind the selected study period growing season (May-July) of 2009. Country based total wheat production data for 2009 were obtained from Food and Agriculture Organizations (FAO). Spatial distribution of country based total wheat production data was performed by using gridded global wheat production map (for year 2000) from studies of Monfreda et al. (2008) and Ramankutty et al. (2008). For each grid cell countries contain a total value was found. These totals then divided by number of grid cells countries contain and grid cell ratios were calculated. These ratios were multiplied with total wheat production data of FAO 2009 and spatially distributed. This created map then remapped according to model area and resolution. In this study, modeling method is WRF / CMAQ modeling system with 30 km spatial resolution. As Meso-scale Atmosphere Circulation Model, WRF-ARW 3.6 (Weather Research and Forecast-Advanced Research WRF) was used with 35 horizontal levels, and with 191 cells in east-west and 159 cells in north-south direction. Also, 0.75 degree ECWMF Era-Interim Reanalysis data was used to prepare initial and boundary conditions of the model. For land-use, MODIS-30 20-class data was prepared. DUMANv2.0 emission model (developed by Istanbul Technical University, Eurasia Institute of Earth Science) was used for emission modeling. Inputs of emission model were anthropogenic, biogenic, and fire emissions. Anthropogenic emissions are created from TNO-2009 database by using DUMANv2.0 with CB05-AERO5 chemical mechanism. MEGAN v2.10 biogenic emission model was used for biogenic emissions. Fire emissions were calculated by data obtained from GFASv1.0 satellite dataset. CMAQv4.7.1 model with CB05-AERO5 chemical mechanism was used for chemical transportation modeling. WRF outputs were converted into M3MODEL structure by using MCIP (Meteorology-Chemistry Interface Processor). ICON (Initial Cond.) and BCON (Boundary Cond.) were used to create initial and boundary conditions. Inputs for these modules were obtained from ECMWF – MACC 3-hour model output with spatial resolution of 80-100 km. Open sky photolysis data were prepared with JPROC (Photolysis Rate Processor).

Ozone variable was obtained from CMAQv4.7.1 model and applied to three ozone exposure indices. Gridded map of wheat production map of 2009 were multiplied with these values, thus calculated the wheat loss in each cell. Total economic loss was calculated by multiplication of calculated production loss and FAO 2009 country based wheat production price index. In order to calculate economic loss between countries, each country's 2009 GDP was normalized.

The highest wheat loss was found in Russia (7.14 Mt - 11.6% and 17.3 Mt – 28%) by AOT40 and M7 methods while W126 method found the highest loss in Italy (1.54 Mt-24%). Following countries generally have higher wheat loss in every method, Turkey (6.8 Mt), France (3.47 Mt), Germany (2.45 Mt), and Egypt (5.54 Mt). According to the regional results the highest loss was found in South (8.3 Mt – 61%) and East (12.8 Mt – 37%) Europe, the lowest loss was found in Northern European countries (2.2%- 0.65Mt). Greatest losses were found in M7 method while W126 method has the lowest loss values. This provides a range (min-max) for ozone caused wheat loss in Europe. The highest economic loss was in Russia with 2.23 billion American Dollar (USD). Turkey (\$2.24 bn), Italy (\$1.64 bn), and Egypt (\$ 1.59 bn) were other countries with high economic loss, right after Russia. Eastern Europe has the highest regional economic losses with (\$1.6 bn) USD and Southern Europe (\$2.8 bn). The lowest economic loss was in Northern Europe (\$0.01 bn). Reason behind the high wheat loss values in Southern and Eastern Europe region is due to ozone precursor transport from Middle – Western European region via southerly – easterly meteorological systems. This causes higher ozone concentrations in Southern and Eastern Europe and affect wheat loss. Emission regulations should be more focused and applied in Middle – Western European countries.





# **WRF/CMAQ MODELLEME SİSTEMİ İLE HAVA KİRLİLİĞİNDEN KAYNAKLANAN AVRUPA'DAKİ TARIMSAL ZARARIN İNCELENMESİ**

## **ÖZET**

Avrupa nüfusu – Avrupa Birliği üyesi olmayan ama kıtasal Avrupa’da yer alan ülkelerle birlikte – 740 milyon civarındadır. Bu dünya nüfusunun %10’una denk gelmektedir (United Nations-UN, 2015). Ayrıca, Avrupa’nın 1996 – 2014 yılları arası toplam buğday üretim miktarı ortalaması 133.9 milyon metrik ton olduğu görülmektedir. Dünya buğday üretiminin %21’ne karşılık gelmektedir (FAO,2015). Buna ek olarak, Endüstri Devrimi’nin Avrupa’da gerçekleşmesinin bir sonucu olarak, bölgenin hava kirliliğinde ve kirletici emisyonlarında günümüze kadar bir artış gözlemlenmiştir. Bu artış beraberinde ciddi çevresel etkileri getirmektedir. Avrupa’da insan sağlığı üzerine yapılan çeşitli çalışmalar ile ozon etkisi tespit edilse de, tarım üzerine odaklanmış çok fazla çalışma bulunmamaktadır. Yüksek Ozon konsantrasyonuna maruziyet, insan sağlığına olan zararlı etkilerinin yanı sıra gıda güvenliğine ve tarımsal aktivitelere ciddi etkileri gözlemlenmiştir.

Yüksek ozon konsantrasyonu ve ozon konsantrasyonundaki değişimler, fotosentez, terleme ve gaz alışverişi gibi bitki yaşam fonksiyonlarını ciddi şekilde etkilemektedir. Literatürde birçok çalışma, yüksek ozon konsantrasyonundan dolayı bitkilerin alt stoama çeperinin, hücre zarı ve duvarlarının zarar gördüğünü göstermiştir. Bu zarar fotosentez hızını düşürmektedir. Bu durum bitki büyümesi hacim ve kütle olarak azalmasına neden olmaktadır. Avrupa’da ve Amerika Birleşik Devletleri’nde (USA) bir çok farklı deneysel ve gözlemsel çalışmalar yapılmıştır. Bu çalışmalar sayesinde dünyanın farklı bölgelerinde daha iyi çalıştığı düşünülen ampirik ozon maruziyet denklemleri üretilmiştir. Tarımsal üretim kayıpları bu ve bunun gibi denklemler sayesinde hesaplanabilmektedir. Avrupa’da yapılan deneysel çalışmalar neticesinde AOT40 – 40 ppb’den yüksek ozon konsantrasyonlarının farkının kümülatif toplamı – yöntemi yaygın olarak kullanılmaktadır. USA’da ise W126 yöntemi USEPA tarafından önerilmektedir. W126 yöntemi sigmoidal dağılım fonksiyonunu kullanarak ozon konsantrasyonlarına ağırlık ataması yapıp gün ışığı süresince olan toplamı almaktadır. Bu iki yöntem dışında belirli eşik değerlerinin farkının günlük toplam şeklinde hesaplanması (SUM-X yöntemi) veya günlük ortalama şeklinde hesaplanması (M-X yöntemi) gibi bir çok yöntemde ozondan kaynaklı tarımsal üretim kaybının hesaplanmasında dünya çapında kullanılmaktadır.

Dünyanın çeşitli yerlerinde yapılan çalışmalar ozonun buğday, soya fasulyesi, pirinç patates gibi tarım ürünlerinin üretiminde ve veriminde kayıplar olduğu söylemiştir. USEPA tarafından 1996 yılında USA için yapılan bir çalışmada yüksek ozon konsantrasyonuna maruz kalması sebebiyle tarımsal üretimde %10 için kayıp olduğu tespit edilmiştir. Benzer bir çalışma bu kaybın Avrupa %5 civarında olduğu göstermektedir. Küresel ve bölgesel bir problem olarak ozon, bitkiler üzerindeki bu etkisi sebebiyle günümüzdeki ve gelecekteki gıda güvenliğini tehdit etmektedir.

Literatürde dünyanın çeşitli bölgelerinde ozonun çeşitli tarım ürünleri üzerindeki etkisini ölçümler ile inceleyen çalışmalar mevcuttur. Bu çalışmalar lokal kaybı gösterse de bölgesel etkiyi göstermekte yayıftır. Bu yüzden bölgesel veya küresel olarak modelleme yöntemi ile üretim kaybı hesaplayan bilimsel çalışmalar literatürde bulunmaktadır. Küresel model yaklaşımı yapılan çalışmaların yersel çözünürlüklerinin düşük olması, elde edilen sonuçların temsiliyetini etkilemektedir. Bölgesel çalışmalarda ise çözünürlük iyi olmasına rağmen, tarım üretim kaybı hesabı hemen hemen hiç bir çalışma da hesaplanmamıştır. WRF/Chem bölgesel kimyasal taşınım modeli ile Hindistan için yapılan bir çalışmada 2005 yılında ozondan kaynaklı buğday üretim kaybı 5 milyon metrik ton olarak hesaplanmıştır. Yine benzer bir çalışmada Eta-CMAQ modeli ile USA'daki soya fasulyesi üretim kaybı 1.7 – 14.2 % olarak hesaplanmıştır. Ozonun bölgesel değişimi sebebiyle bölgesel kimyasal model ile çalışmak hesaplanan tarımsal üretim kaybındaki belirsizliği azalmaktadır. Küresel modellerde yüzeyin tanımlanması, yersel çözünürlüğün düşük olması gibi birden çok belirsizlik söz konusudur.

Bu çalışmada WRF/CMAQ model sistemi ile Avrupa'daki Buğday üretim kaybının üç farklı ozon maruziyet denklemi (AOT40, W126 ve M7) kullanılarak belirlenmiştir. Bunu için öncelikle buğday bitkisini büyüme mevsimi (Avrupa için Mayıs – Temmuz ) literatüre göre tespit edilmiştir. Avrupa Çevre Ajansı (European Environmental Agency - EEA) AirBase veri tabanı ozon gözlemleri 2008 -2012 yılları büyüme mevsimleri ortalamaları hesaplanmış ve incelenmiştir. En yüksek buğday büyüme mevsimi ortalaması (45.6 ppb) 2009 yılında bulunmuştur. Bu değer 2008 yılında 33.28 ppb, 2010 yılında 29.29 ppb, 2011 yılında 39.12 ve 2012 yılında 30.42 ppb olarak hesaplanmıştır. Bu yüzden çalışma dönemi olarak 2009 büyüme mevsimi (Mayıs - Temmuz) seçilmiştir. Çalışmada Food and Agriculture Organizations (FAO)'dan seçilen yıl 2009 için ülke bazlı toplam buğday üretim verisi temin edilmiştir. Ülke bazlı toplam buğday üretim verilerinin yersel dağılımı ise Monfreda vd. (2008) ve Ramankutty vd. (2008) çalışmalarında yayınlanan küresel ve gridlenmiş 2000 yılı için buğday üretim haritası kullanılarak yapılmıştır. Bunun için ülkelere düşen her grid hücresinin ülke bazlı toplamı alınmıştır. Hesaplanan toplamlar, grid hücrelerindeki değerlere bölünerek her bir hücrenin oranı belirlenmiştir. Bu oranlar FAO 2009'dan temin edilen toplam buğday üretim verisi ile çarpılarak 2009 yılı FAO buğday üretim verileri yersel olarak dağıtılmıştır. Hazırlanan harita, model alanı ve çözünürlüğüne göre yeniden haritalandırılmıştır. Çalışmada modelleme yöntemi olarak WRF / CMAQ model sistemi 30 km yersel çözünürlükle kurgulanmıştır. Mezo-ölçek Atmosfer Sirkülasyon Modeli olarak WRF-ARW 3.6 (Weather Research and Forecast-Advanced Research WRF) modeli, düşeyde 35 seviye, doğu-batı yönünde 191 ve kuzey-güney yönünde 159 hücre ile çalıştırılmıştır. Ayrıca 0.75 derece ECWMF Era-Interim Reanalysis verisi modelin başlangıç ve sınır koşullarının hazırlanması için kullanılmıştır. Yüzey kullanımı için MODIS-30s 20-Sınıf verisi hazırlanmıştır. Emisyon modellemesi, İTÜ Avrasya Yer Bilimleri Enstitüsü tarafından geliştirilen DUMANv2.0 modeli kullanılarak yapılmıştır. Emisyon modeline insan kaynaklı, biyogenik ve yangın emisyonları girdi olarak verilmiştir. İnsan kaynaklı emisyonlar, TNO-2009 veri tabanından elde edilmiş ve DUMANv2.0 tarafından CB05-AERO5 kimyasal mekanizmasına göre işlenmiştir. Biyogenik emisyonlar için MEGAN v2.10 kullanılmıştır. Yangın emisyonları ise literatürde yer alan ve GFASv1.0 uydu veri setinden elde edilen bilgilerle hesaplanmıştır. Kimyasal Taşınım modeli olarak CMAQv4.7.1 modeli CB05-AERO5 kimyasal mekanizmasına göre

çalıştırılmıştır. İlk olarak WRF çıktıları MCIP (Meteorology-Chemistry Interface Processor) kullanılarak M3MODELS yapısına çevrilmiştir. ICON (Initial Cond.) ve BCON (Boundary Cond.) modülleri kimyasal başlangıç ve sınır koşullarını oluşturmak için çalıştırılmıştır. Bu modüllere girdi bilgisi ECMWF – MACC 3 saatlik model (yersel çözünürlüğü 80-100 km) çıktılarından sağlanmıştır. JPROC (Photolysis Rate Processor) ile açık gökyüzü şartlarındaki fotoliz bilgisi hazırlanmıştır.

CMAQv4.7.1 modelinden ozon değişkeni temin edilmiş ve belirlenen üç ozon maruziyet denklemlerine uygulanmıştır. Hazırlanan 2009 yılı için gridlenmiş buğday üretim haritası ile çarpılarak her hücredeki buğday kaybı hesaplanmıştır. Bu kayıplar ile FAO'dan 2009 yılı için alınan ülke bazlı buğday üretici fiyat indeksi çarpılarak her bir ülkenin toplam ekonomik kaybı hesaplanmıştır. Ülkeler arası ekonomik kaybı hesaplayabilmek için her ülkenin 2009 yılı için GDP'si ile normalize edilerek yorumlanmıştır.

Buna göre, en yüksek buğday kaybı AOT40 ve M7 yöntemleri ile Rusya'da (7.14 Mt - %11.6 ve 17.3 Mt %28), W126 yöntemi ile İtalya'da (1.54 Mt-%24) hesaplanmıştır. Genel olarak kaybın tüm yöntemlerde yüksek görüldüğü diğer ülkeler, Türkiye (6.8 Mt), Fransa (3.47 Mt), Almanya (2.45 Mt) ve Mısır (5.54 Mt)'dir. Bölgesel olarak kayıplar incelendiğinde ise tüm yöntemler içinde en yüksek Güney (8.3 Mt - %61) ve Doğu (12.8 Mt – %37 ) Avrupa'da, en düşük bölge ise kuzey Avrupa ülkeleri (%2.2- 0.65Mt) olduğu belirlenmiştir. En yüksek hesaplanan kayıplar M7 yönteminde, en düşük kayıplar ise W126 yöntemi ile yapılan hesaplamada bulunmuştur. Bu sonuç Avrupa'da ozondan kaynaklı buğday kaybı hakkında bir aralık (minimum - maksimum) sunmaktadır. En yüksek ekonomik kayıp Rusya'da 2.23 Milyar Amerikan Doları (USD) olarak hesaplanmıştır. Türkiye (\$2.24 Milyar), İtalya (\$1.64 Milyar), Mısır (\$ 1.59 Milyar) Rusya'yı takip etmektedir. Hesaplanan ekonomik kayıplara göre, en yüksek kayıplar Doğu (\$1.6 Milyar) ve Güney (\$2.8 Milyar) Avrupa ülkelerinde, en düşük ekonomik zarar yine Kuzey Avrupa ülkelerinde (\$0.01 Milyar) görülmüştür. Güney ve Doğu Avrupa'da bu derece yüksek kayıpların çıkması, Merkez ve Batı Avrupa ülkelerindeki endüstriden kaynaklı ozon öncül kirleticilerin güney ve doğu yönlü meteorolojik sistemlerle taşınmasıdır. Bu sebeple Avrupa'nın güneyinde ve doğusunda ozon yüksektir ve buğday kaybı bundan dolayı daha yüksek hesaplanmıştır. Emisyon kontrolleri Batı ve Merkez Avrupa ülkelerinde daha yoğun şekilde uygulanmalıdır.



## 1. INTRODUCTION

Ozone is a secondary air pollutant in the atmosphere and it acts as a short-lived climate forcer. Hence it has a significant role on regional and global climate. According to IPCC tropospheric O<sub>3</sub> has climate forcing potential of 0.4 W/m<sup>2</sup>. Only a small volume of atmospheric ozone (O<sub>3</sub>) is located close to the earth's surface, in troposphere. Tropospheric ozone is formed by photochemical reaction of primary pollutants mainly nitrogen oxides (NO<sub>x</sub>), volatile organic compounds (VOCs) in the presence of sunlight (Crutzen, Lawrence, & Poschl, 1999). Concentration of ozone is highly dependent on meteorological conditions. Specifically, ozone rises to critical concentration values in summer months due to large amount of sunlight and prevailing high-pressure system. Higher surface temperatures in urban areas may have a positive feedback in chemical reaction rates (Pleijel, 2007).

There is an increasing trend in ozone precursors emitted from both anthropogenic and biogenic sources, which, in turn, drives up tropospheric ozone concentration values higher than the pre-industrial era concentrations (Lamarque et al., 2010). In the 19<sup>th</sup> century, ozone studies were focused on to prove its existence, and its reactions in the atmosphere and interactions with human health. Ozone measurements began in the mid-1800s with more than 300 stations around the world, however, a few of them made measurements continuously (Vingarzan, 2004). Because of this, observation of ozone in the end of 19<sup>th</sup> century is extremely limited. Pavelin, Johnson, Rughooputh, and Toumi (1999) reported that reconstructed ozone measurements made with traditional methods show the variability of O<sub>3</sub> between 5 – 15 ppb for the mid-19<sup>th</sup> century. Observational network of tropospheric O<sub>3</sub> is increased during 20<sup>th</sup> century. In the last decades, the ozone observation network and newer methods have been developed to make more accurate/precise O<sub>3</sub> measurements to understand the global O<sub>3</sub> distribution (Fishman, Watson, Larsen, & Logan, 1990; J. Logan, 1999; Thouret et al., 2006; Vingarzan, 2004). Vingarzan (2004) showed that annual range of mean ozone at background measurement sites around the world varies within 11 – 46 ppb range

between the years 1989 – 2001. Comparing background ozone levels for late-19th and early-20th centuries indicates that current ozone levels has increased approximately twice (Bozo & Weidinger, 1995; Staehelin, Thudium, Buehler, Volz-Thomas, & Graber, 1994; Cartalis & Varotsos, 1994).

Some of the ozone studies have been conducted to understand variability of O<sub>3</sub> and analyze the changes via observational O<sub>3</sub> dataset (Cooper et al., 2010; J. A. Logan et al., 2012; Parrish et al., 2012; Oltmans et al., 2013). These studies show that there is good indication of increasing O<sub>3</sub> around 1 percent between the years 1950 -2000 at mid-latitudes in Northern Hemisphere. They have also reported that the increase has slowed down over the last decade, this might be related to emission control efforts. Although the changes in emissions are the basic driver of the O<sub>3</sub> change, other several factors and parameters have contribution to forming O<sub>3</sub>. Oltmans et al. (2006) indicate that one of the largest changes in tropospheric ozone is seen in Europe, Zugspitze station (Germany) with an overall increase of 12.6 ( $\pm$  0.8) percent per decade. Although surface ozone significantly increases during all months, the largest increase is in spring and summer months (Figure 1.1). According to report of the Royal Society (2008), tropospheric ozone trends show an upward trend of 0.2 – 0.5 ppb per year over the period of 1992- 2001 (Figure 1.2). There seem to be an obvious upward trend but the trend slopes differ from region to region (J. Logan, 1999; Jen, 2008). Similar results were obtained by global model studies for historical, current, and future tropospheric ozone (Young et al., 2013; Stevenson et al., 2013).

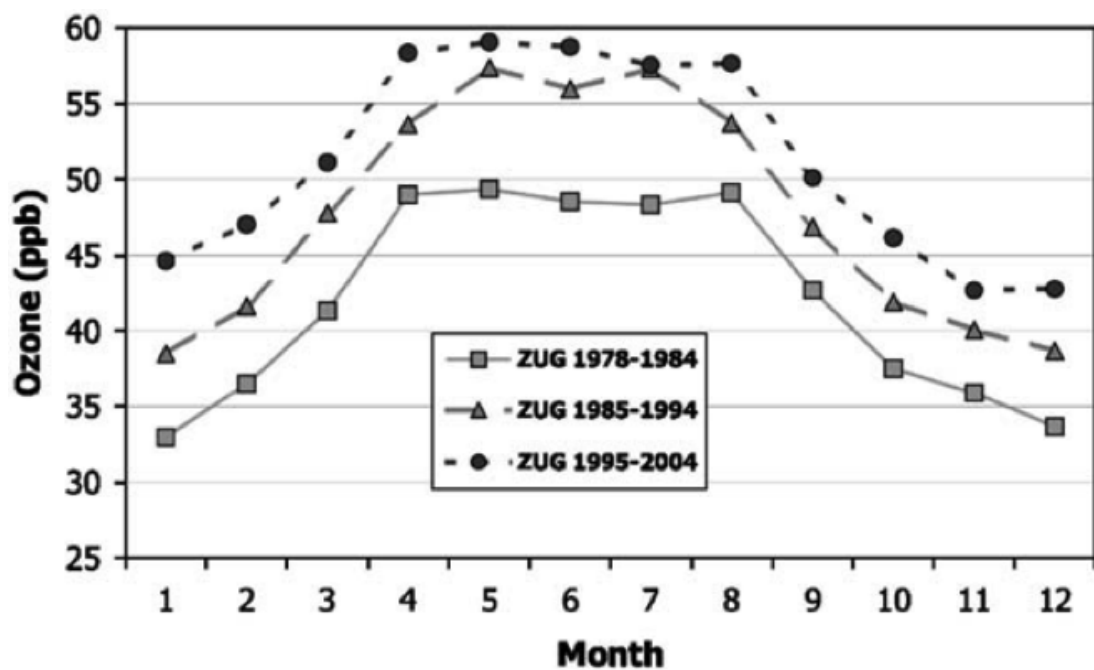


**Figure 1.1** : Average Monthly Surface Ozone at Zugspitze station, Germany(Oltmans et al., 2006).

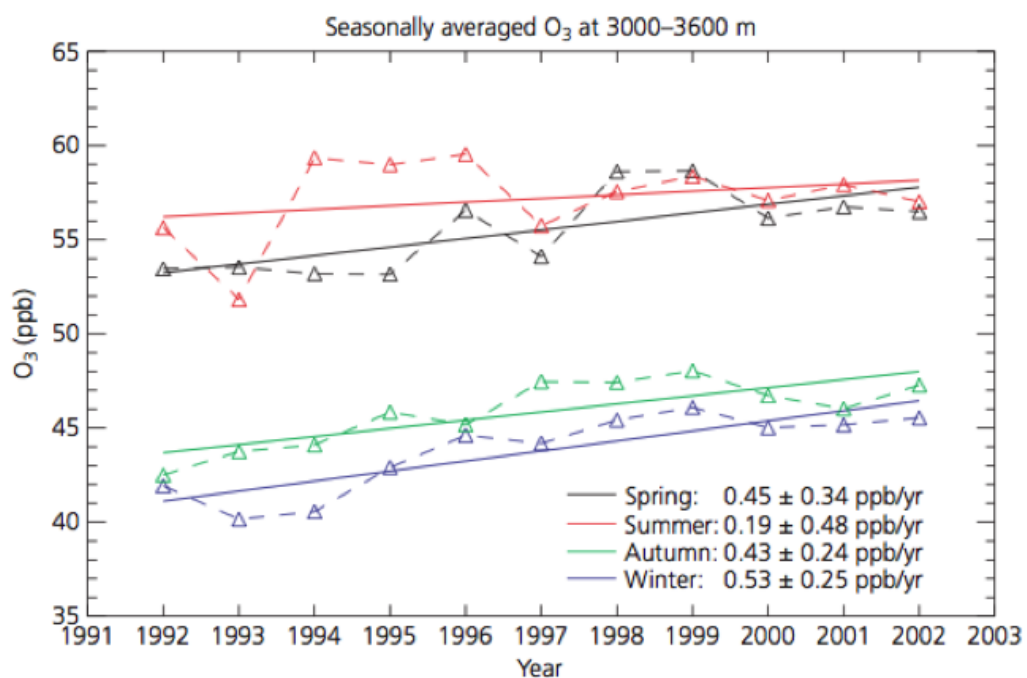


**Figure 1.2** : Time series of seasonal mean O<sub>3</sub> concentrations at three European mountain locations, Jungfraujoch, Zugspitz and Sonnblick (Royal Society, 2008).

Elevated O<sub>3</sub> concentrations and changes in the concentrations may affect plant life functions such as photosynthesis, transpiration, and gas exchanges. It has been found by many scientific studies that ground-level ozone exposure reduces photosynthesis of crops since it damages substomatal apoplast, cell membranes and walls (Figure 1.3). Decreased photosynthesis results in low growth rates in terms of volume or biomass (Reich & Amundson, 1985; Wilkinson, Mills, Illidge, & Davies, 2011). In addition, ozone can cause internal cell damage to plants by entering through the stomata of the plant during the gas exchange in the daylight time. Ozone dissolves inside the plants and starts a chain reaction of oxidation causing a number of problems and distorts plant metabolism. However, due to the transboundary and complex nature of formation and effects of ozone, it is a global problem that threatens not only vegetation but human health and food security.

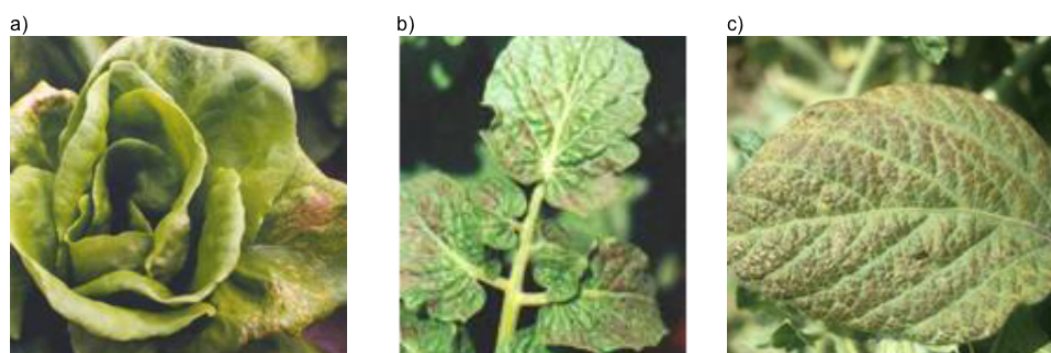


**Figure 1.3 :** Ozone injury on (a) white clover, (b) brown knapweed and (c) violet

There are several experimental and observational studies conducted to determine the impacts of ozone on agricultural crops (Figure 1.4), their yield losses and relative yield losses for different parts of the world (Hunova, Livorova, & J., 2003; Wang & Mauzerall, 2004; Morgan, Mies, Nelson, & Long, 2006; Malley, Heal, & Mills, 2015). Figure 1.5 from a study by Heck et al. (1983) shows the reduction in yield of crops exposed to ozone. At an ozone concentration of 60 parts per billion, soybeans yields decrease to about 75 percent of normal, while wheat, corn, and alfalfa yields decrease to about 90 percent of normal.

Two studies (Debaje, 2014; Sinha & Sangwan, 2015) were conducted on effects of ozone on agricultural production in India. Results of these studies indicated an estimated wheat and rice production losses due to ozone exposure. In one of the studies (Debaje, 2014), two ozone exposure metrics were used and results of this study found 9





**Figure 1.4 :** The more wheat is exposed to ozone pollution, the more its growth is reduced, even if the plants grow in a part of the world far away from the source of pollution. Photographer: Abdul Wahid, Pakistan

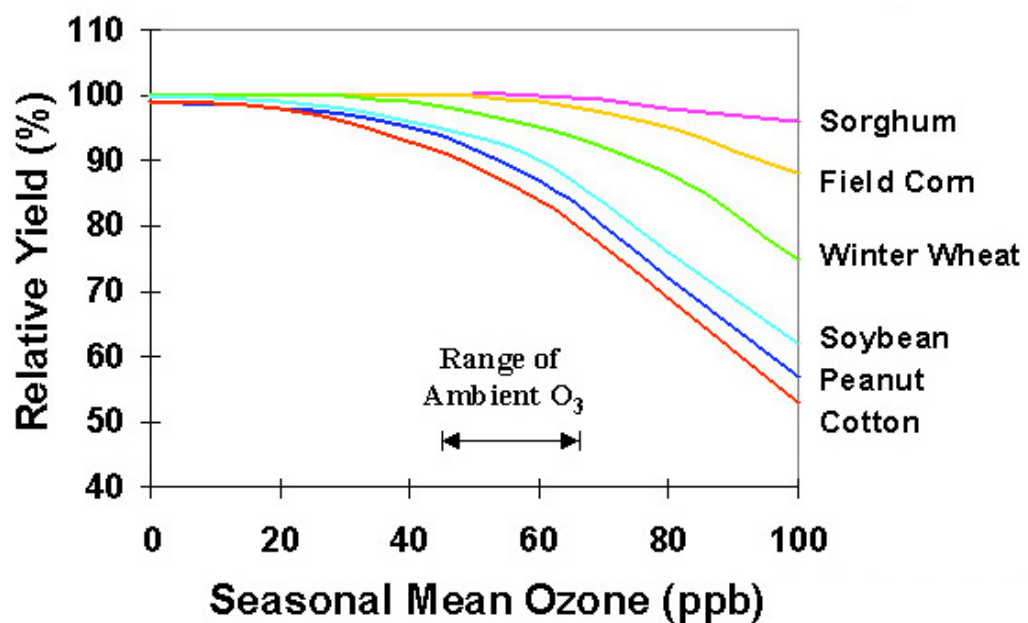


**Figure 1.5 :** The Relationship between Ozone and Relative Yield for six agricultural products

to 29 Mt loss in wheat production and 0.64 to 2.1 Mt loss in rabi rice production. In the other study, wheat production loss was calculated as 20.8 Mt and 10.3 Mt for the State

of Punjab and Haryana in India for the fiscal years of the 2012-2013 and 2013-2014, respectively, while rice production loss was calculated to be 5.4 Mt and 3.2 Mt for the same period (Sinha & Sangwan, 2015). A similar study for the EU found that the loss could be around 5 percent (Krupa, Nosal, & Legge, 1998) whereas, USEPA (1996) has estimated 10 percent crop loss due to ozone in the US.

In the above studies, only ground ozone observation data were used. However, number of stations used in those studies never exceeded 90 stations for regional investigations. Although, the data obtained from stations are good at representing the local effects, they might fail to represent regional effects. For this purpose, many scientific studies focused on quantifying the impact of ozone pollution on crops used regional or global atmospheric models. Van Dingenen (2009) estimated the ranges of wheat production losses by using a global model at the resolution around 100 km x 100 km. Wheat production losses were estimated as 45-81 Mt for the world and 5.3-6 Mt for EU25 countries. In the same study, economic losses were predicted as 6.3 - 12 Billion USD for the world and 0.6 - 0.65 Billion USD for the year of 2000.

In a study, a global model at 2.8° resolution were used to calculate a production loss of 21-93 Mt of wheat, 13-32 Mt of maize and 15-36 Mt of soybean worldwide, which correspond to 4 -15 percent of wheat, 2.2-5.5 percent of maize and 8.5 – 14 percent of soybean production (Avnery, Mauzerall, Liu, & Horowitz, 2011). In an another study conducted by Wang and Mauzerall (2004), at a resolution of 2.8x2.8°, found that 1-9 percent of wheat, rice and corn, 23-27 percent of soybean in China, Japan and South Korea were lost for the year of 1990. Similar study conducted by Hollaway, Arnold, Challinor, and Emberson (2012) indicated that 100 percent NO<sub>x</sub> emission reduction in North America has the highest transboundary effect showing the crop production loss of 14.2 to 63.2 percent in Europe.

Tong et al. (2009) used Eta-CMAQ regional chemical transport model to estimate the soybean loss, and found that amount of loss was in range of 1.7-14.2 percent for the year of 2005 in U.S. This study includes the amount of the crop production loss by using several ozone crop exposure indices some of which are also used in our study. Results of a regional modeling study by Roy, Beig, and Ghude (2009) showed AOT40 values exceeding the threshold in a large area of India, resulting in 5 percent reduction

in the yield of many crops. Ghude et al. (2014) found wheat was the most affected crop with 3.5 Mt loss (5 percent) and 0.62 Billion USD by using WRF/Chem regional chemistry model. Although both studies by Roy et al. (2009) and Ghude et al. (2014) have estimations for crop production loss, their spatial resolutions were not sufficient to solve O<sub>3</sub> concentrations. Tropospheric O<sub>3</sub> shows variability depending on topography making it necessary to use a regional chemistry model to solve this variability. Impact of grid resolution on air quality model is well established, especially in O<sub>3</sub> estimation (Stroud et al., 2011; Arunachalam, Wang, Davis, Baek, & Jonathan, 2011; Cohan, Hu, & Russell, 2006)

### **1.1 Objective**

The population of Europe including non-EU countries (placing in Europe) was predicted to be 740 million, corresponding to 10 percent of the world population. According to EU countries the population was seemed as 508 Million (United Nations (UN), 2016). Also, wheat production in between 1996-2014 in Europe constitutes 21 percent (133.9 Mt) of world's wheat production according to FAO database (Food and Agriculture Organizations (FAO), 2016). Additionally, Europe is the place where the industrialization is relatively high, which resulting in more tropospheric O<sub>3</sub> variability. However, there are not many studies focus on the impact of ozone on agriculture in Europe.

We have utilized a regional chemical transport model as well as monitoring data to quantify wheat production loss over Europe. In order to determine the wheat production loss, due to tropospheric ozone and its economic impacts for Europe and its surrounding areas, three different ozone crop exposure indices (AOT40, W126, and M7) were applied. These three ozone exposure indices were evaluated using ozone concentration values produced by WRF/CMAQ high-resolution modeling system (30 km). Global wheat production gridded data was obtained from datasets published by Ramankutty, Evan, Monfreda, and Foley (2008) and Monfreda, Ramankutty, and Foley (2008), and it was modified accordingly to FAO 2009 country-specific wheat production (Figure 1.6). Total production losses were calculated using ozone exposure indices on country and regional basis. Economic losses were determined using country-specific producer prices, which are taken from FAO Food Statistics

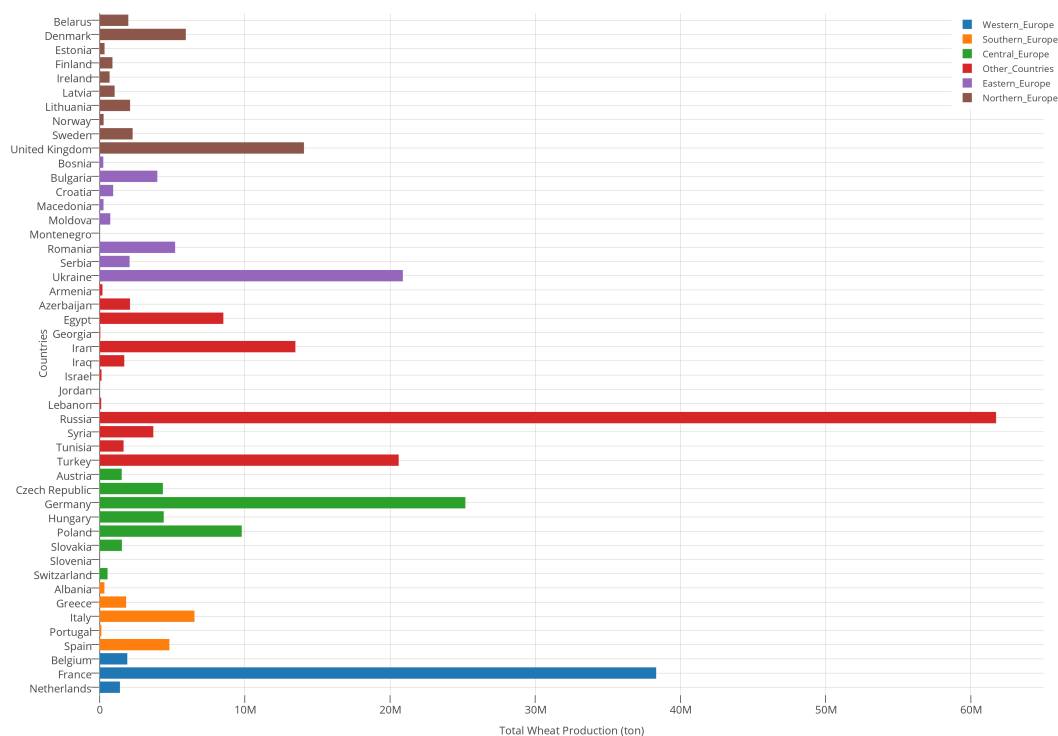


**Figure 1.6 :** Country Specific Total Wheat Production for the year of 2009 over continental Europe

Division. Same analysis were repeated with ozone observations obtained from European Environmental Agency (EEA) AirBase database (version 8).

## **2. DATA & METHODOLOGY**

### **2.1 Ozone Observations and Study Period**

Ozone observations were provided by AirBase database which is the European Air Quality Database managed by European Environment Agency (EEA). The database was prepared with air quality monitoring stations' data operated by the member states of European Union (EU). AirBase includes daily or hourly data from 35 European countries, 140 pollutants, and has more than 6000 stations. Also, it contains information and statistics of monitoring stations presented by the member states of EU. This database was validated by EEA's European Topic Centre on Air pollution and Climate Change mitigation (European Environment Agency (EEA), 2013).

In this study, hourly O<sub>3</sub> data of 1262 stations from AirBase database were used and growing season averages of ozone datasets were calculated for the years 2008-2012 (Figure 2.1-b). It should be noted that the highest average ozone concentration is observed in 2009 (45.59 ppb), which is significantly higher as compared to other years (30.42 for 2012, 39.12 for 2011, 29.29 for 2010, 33.28 for 2008). We have selected the study period for the following of this study as the year 2009 growing season (May-July 2009) because of the highest O<sub>3</sub> concentrations over EU countries. Figure 2.1-a shows that Southern Europe (Italy, Spain, South of France) has the highest (above 45 ppb) growing season ozone averages in the year of 2009. In addition, diurnal cycle of O<sub>3</sub> concentrations in growing season (May-July) and in 2009 were analyzed. According to that, there is big differences (range of 3 - 10 ppb) between May-July and annual hourly ozone concentration profiles, especially in mid-day (Figure 2.2). The wheat production loss was calculated with observed and simulated ozone using ozone exposure indices (AOT40, W126 and M7) for the determined study period. Results of three different indices calculated by observed and simulated ozone were analyzed.

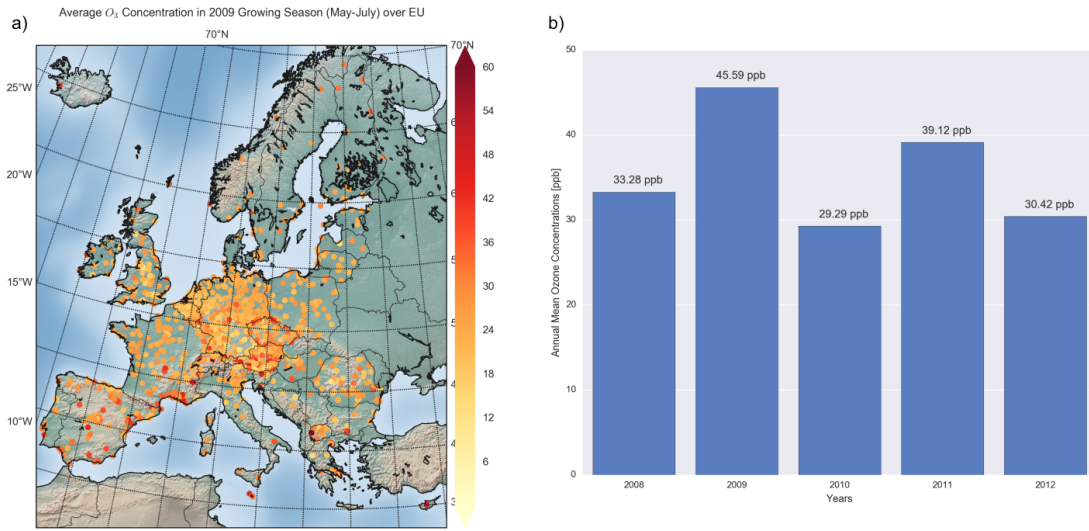


**Figure 2.1 :** Mean Ozone Concentrations During Growing Season of the year 2009 over the Europe

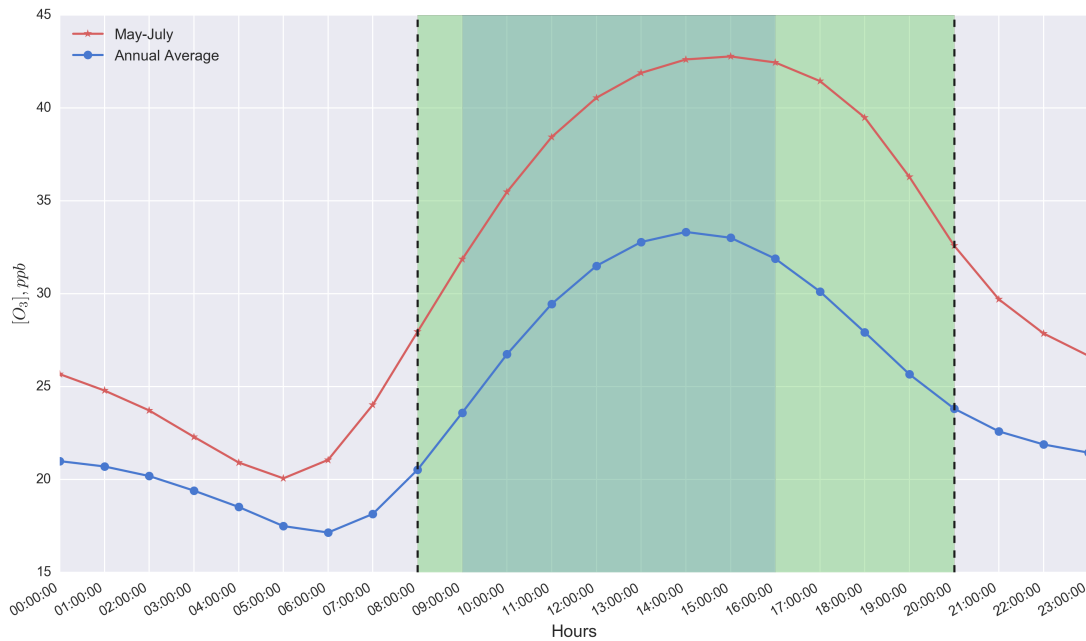


**Figure 2.2 :** Diurnal Cycle of Ozone in growing season of 2009 (May-July) and annual average of 2009

## 2.2 Distribution of the Wheat Production

Country-specific wheat production for the year of 2009 obtained from FAO is used in this study (Figure 1.6). However, this data contains the country total production values, not spatially distributed wheat production. The distribution of the wheat production areas and its yield were mapped by (Monfreda et al., 2008) and (Ramankutty et al., 2008) via statistical data fusion method where two satellite-derived products (Boston

University's MODIS-based land cover dataset and GLC2000 dataset). Also, prepared dataset were combined with national, state and country- level yield statistics. Mapped production datasets were prepared at 5 min x 5 min latitude and longitude spatial resolution for between the years 1997 and 2003. Latest datasets were generated via taking average the determined wheat production (Figure 2.3) and its yield (Figure 2.4) for this period to represent the year 2000 for each country.

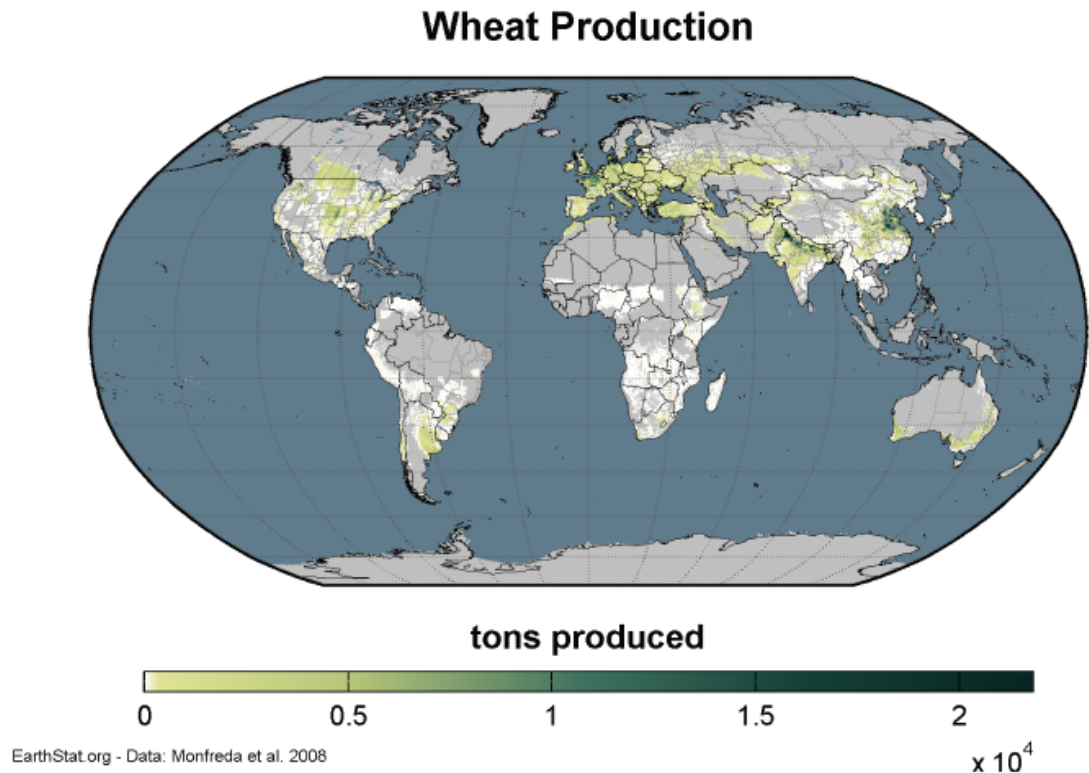


**Figure 2.3 :** Global Wheat Production (ton) for the year 2000

The production ratio in each grid cell has been determined using this dataset and its calculated country total values for the year of 2000. These ratios have been multiplied with FAO country total wheat production to distribute wheat production spatially for the year of 2009 that is study period. Therefore, spatially distributed wheat production information for the year 2000 is converted to FAO 2009 wheat production map. The wheat production distribution has been regridded to 30 km x 30 km resolution that is the modeling system resolution for calculations of yield losses due to ozone exposure (Figure 2.5). The highest production per grid cell is over Nile delta in Egypt as well as North Western Europe. Production per grid cell in Germany and United Kingdom is also higher than other regions over Europe. Wheat planted areas in Russia and Turkey are larger than most of the EU countries that boost the amount of total production. In



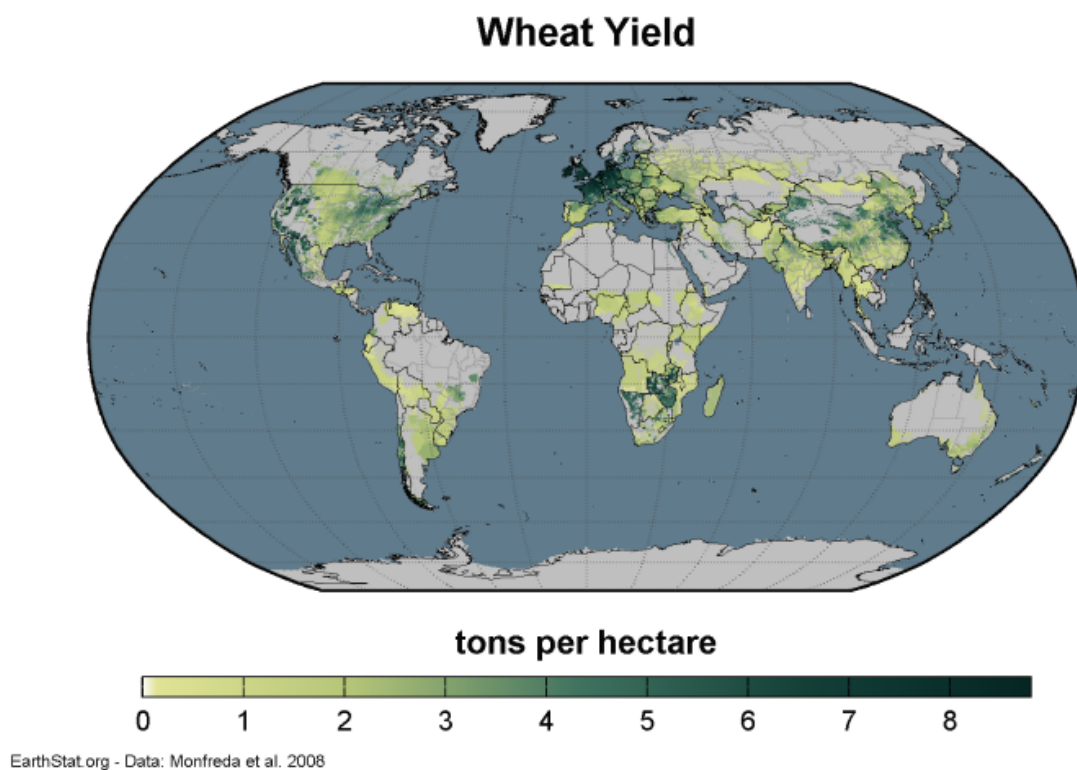


**Figure 2.4 :** Global Wheat Yield per hectare for the year 2000

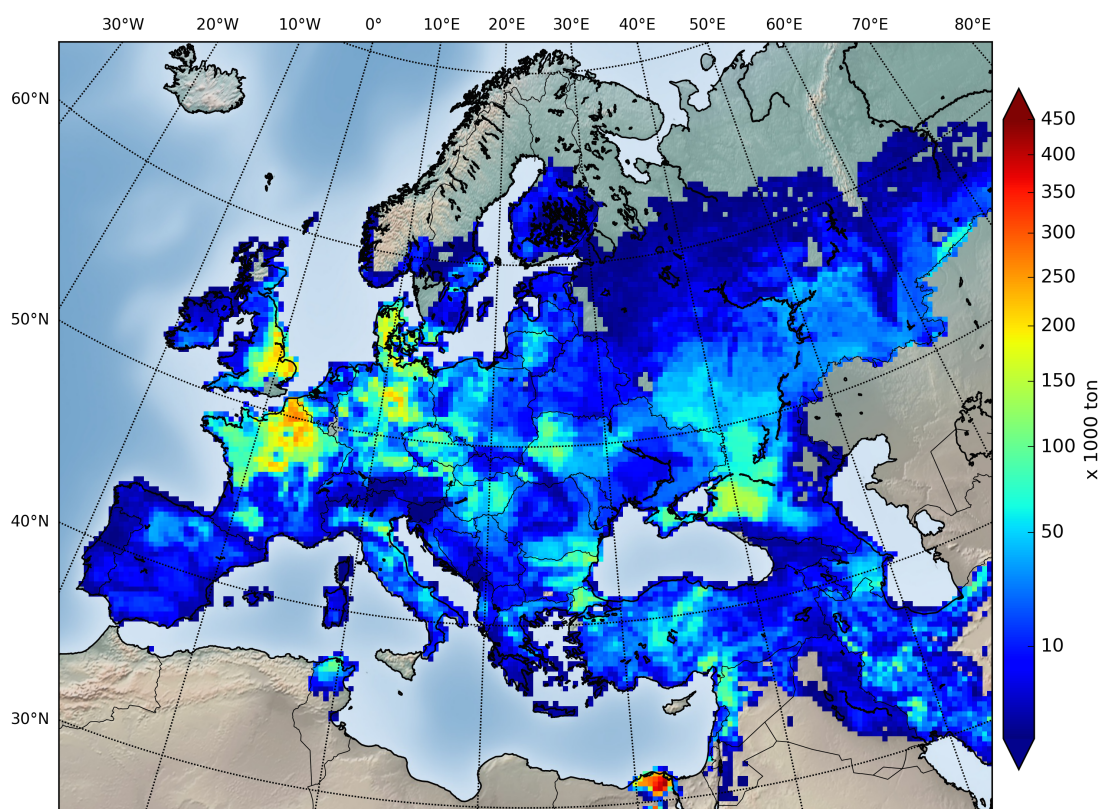


**Figure 2.5 :** Wheat Production for the year of 2009 (FAO based-30 km x 30 km)

addition, the data for the wheat production covered 72 percent of wheat planted area in Russia. The interpretation of the analysis was made according to this condition.



## 2.3 Modeling Framework

Air quality model (AQM) mathematically analyzes atmospheric reactions, transportation and diffusion of pollutants. For air quality modeling purposes, meteorology, emission and chemical reactions are calculated by using thousands of mathematical and physical formulations. A regional scale air quality modeling system which is the US-EPA Community Multiscale Air Quality (CMAQ) model, version 4.7.1 (Foley et al., 2010) coupled with Weather Research and Forecasting model (WRF- ARW v3.6 (Skamarock et al., 2008)) was adopted to assess the ozone impacts on wheat production in this study. The methodology is given in Figure 2.6

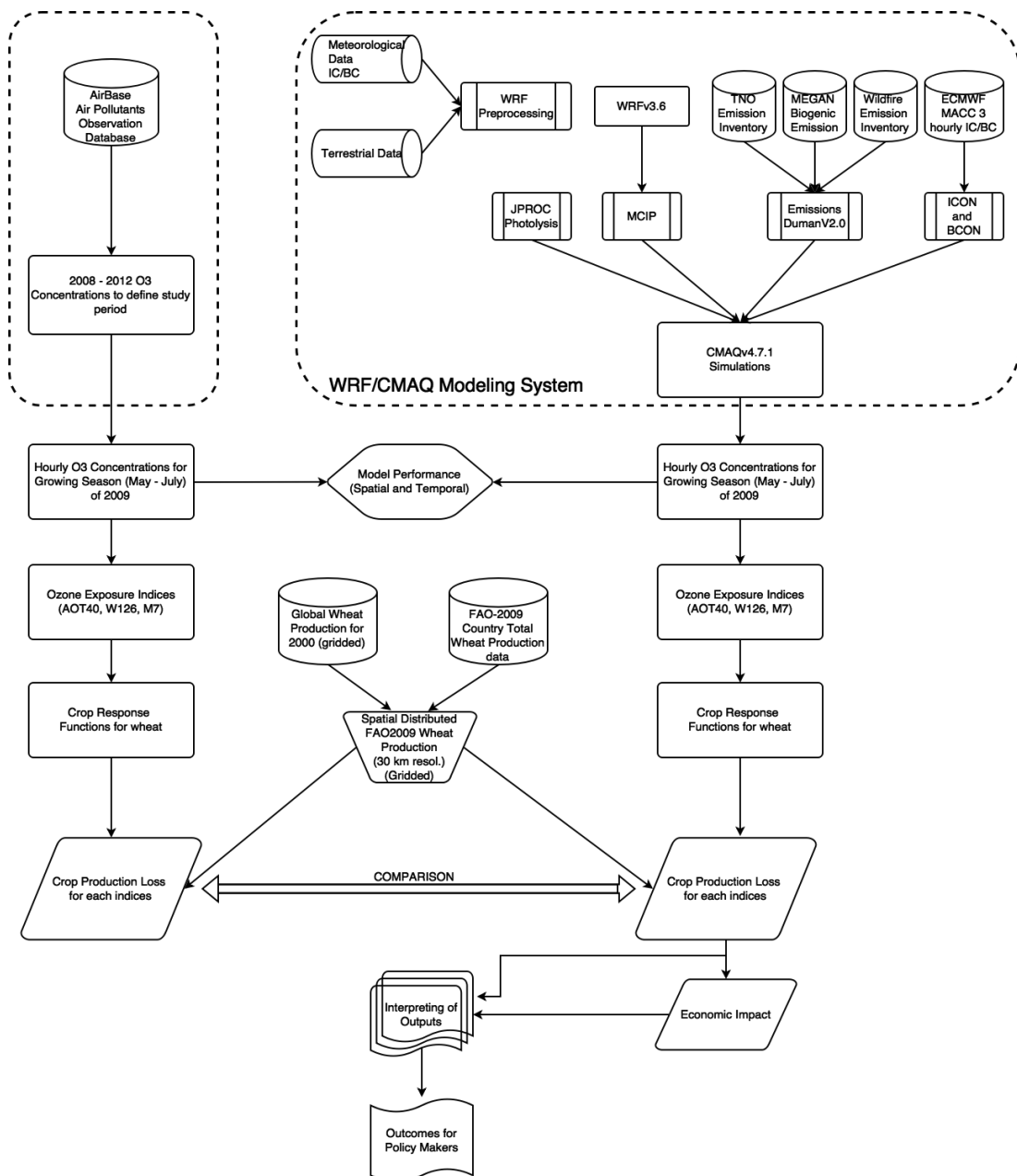


**Figure 2.6 :** Flow Chart of Methodology in the Study

### **2.3.1 Meteorological Modeling**

Meteorological models are built up with all primitive dynamical atmospheric equations and they use these mathematical formulas to simulate atmospheric circulations and processes such as wind, temperature, pressure etc. at a large range of scale. These meteorological variables are calculated at spatially distributed equidistant points which are called grids for an interested area horizontally and vertically. These calculations need high computational time and supercomputer powers. Study area-means modeling domain- and physical parameterizations have to be chosen attentively to make optimization for computational time and supercomputers power. This kind of application –optimizations – may increase the modeling performance and effectiveness of the study. As a popular field, meteorological models are also developing day by day to increase accuracy. With these purposes, WRF-ARW version 3.6.1 was used to simulate meteorological variables need by chemical transport models.

#### **2.3.1.1 Weather Research and Forecast Model (WRF)**

Weather Research and Forecasting (WRF) model is an open-source, regional dynamic and non-hydrostatic numerical weather prediction model. WRF model is systemized and developed by National Center for Atmospheric Research (NCAR), the National Oceanic and Atmospheric Administration (NOAA) groups, the Forecasting System Laboratory (FLS), the Air Force Weather Agency (AFWA), the Naval Research Laboratory, the University of Oklahoma and the Federal Aviation Administration (FAA) collaboration. The model is designed for operational weather forecasting and atmospheric research proposes. It is still getting updates. WRF as a next generation atmospheric model of MM5 has two basic computational cores that are known as ARW (Advanced Research WRF) and NMM (Non-hydrostatic Mesoscale Model). These cores provide to all users a wide range of uses. So, researchers or users may use the model to create real case or ideal case simulations. Additionally, WRF-ARW as a dynamic atmospheric model comes with a lot of physical parameters. Because of wide range of setup options, WRF-ARW is selected to create atmospheric variables.

WRF-ARW has two components, WPS (WRF Preprocessing System) and WRFV3 (numerical core). WPS component is divided into three modules, geogrid, ungrib and

metgrid. WRFV3 component has two modules which are real.exe and wrf.exe. This modeling structure and its flow chart are shown in Figure 2.7.

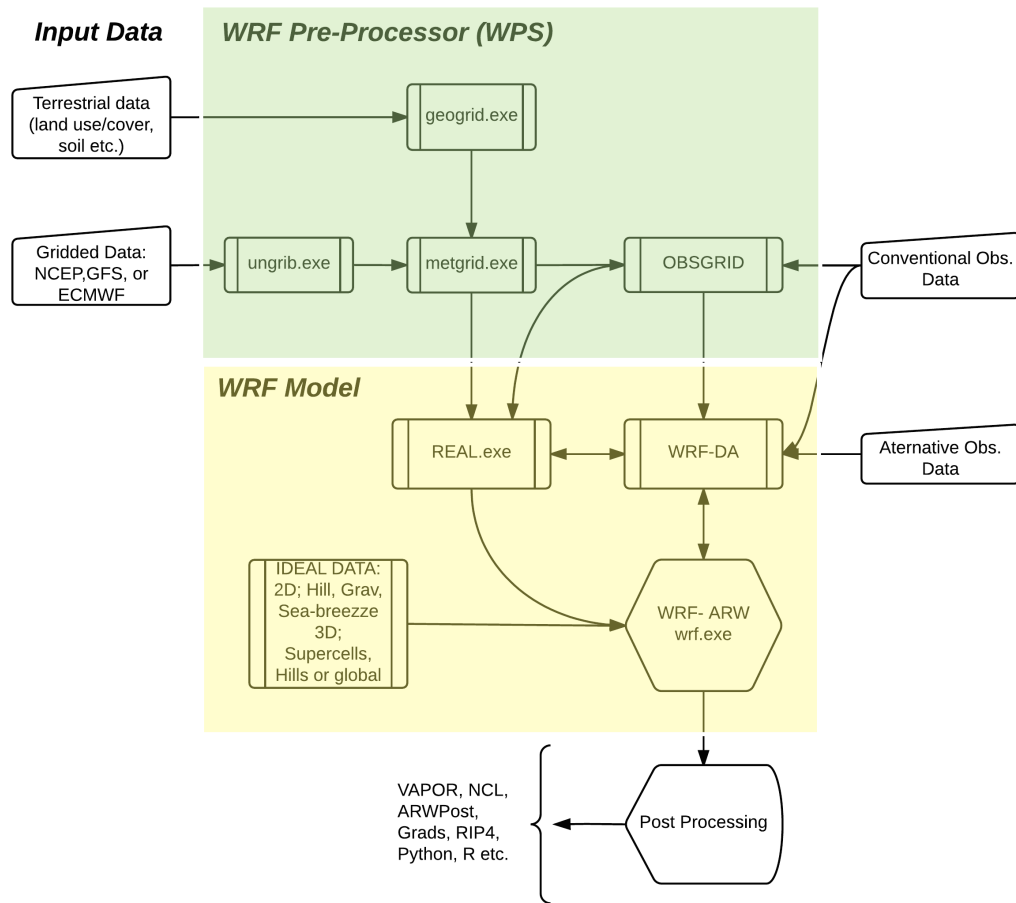


**Figure 2.7 : WRF Modeling System Flow chart**

### 2.3.1.2 WRF-ARW Programs

#### geogrid Module

The purpose of geogrid is to define the simulation domains, and interpolate various terrestrial data sets to the model grids. The simulation domains are defined using information specified by the user in the “geogrid” namelist record of the WPS namelist file, `namelist.wps`. In addition to computing the latitude, longitude, and map scale factors at every grid point, geogrid will interpolate soil categories, land use category, terrain height, annual mean deep soil temperature, monthly vegetation fraction, monthly albedo, maximum snow albedo, and slope category to the model grids by default. Global data sets for each of these fields are provided through the WRF download page. Several of the data sets are available in only one resolution, but others

are made available in resolutions of 30", 2', 5', and 10'; here, " denotes arc seconds and ' denotes arc minutes. The user need not download all available resolutions for a data set, although the interpolated fields will generally be more representative if a resolution of data near to that of the simulation domain is used. However, users who expect to work with domains having grid spacings that cover a large range may wish to eventually download all available resolutions of the static terrestrial data.

Besides interpolating the default terrestrial fields, the geogrid program is general enough to be able to interpolate most continuous and categorical fields to the simulation domains. New or additional data sets may be interpolated to the simulation domain through the use of the table file, GEOGRID.TBL. The GEOGRID.TBL file defines each of the fields that will be produced by geogrid; it describes the interpolation methods to be used for a field, as well as the location on the file system where the data set for that field is located.

### **ungrib Module**

The ungrib program reads GRIB files, "degrib" the data, and writes the data in a simple format called the intermediate format. The GRIB files contain time-varying meteorological fields and are typically from another regional or global model, such as NCEP's NAM, GFS or ECMWF models. The ungrib program can read GRIB Edition 1 and, if compiled with a "GRIB2" option, GRIB Edition 2 files.

GRIB files typically contain more fields than are needed to initialize WRF. Both versions of the GRIB format use various codes to identify the variables and levels in the GRIB file. Ungrib uses tables of these codes – called Vtables, for "variable tables" – to define which fields to extract from the GRIB file and write to the intermediate format. Vtables for common GRIB model output files are provided with the ungrib software.

Vtables are provided for NAM 104 and 212 grids, the NAM AWIP format, GFS, the NCEP/NCAR Reanalysis archived at NCAR, RUC (pressure level data and hybrid coordinate data), AFWA's AGRMET land surface model output, ECMWF, and other data sets. Users can create their own Vtable for other model output using any of the Vtables as a template.

## **metgrid Module**

The metgrid program horizontally interpolates the intermediate-format meteorological data that are extracted by the ungrib program onto the simulation domains defined by the geogrid program. The interpolated metgrid output can then be ingested by the WRF real program. The range of dates that will be interpolated by metgrid are defined in the “share” namelist record of the WPS namelist file, and date ranges must be specified individually in the namelist for each simulation domain. Since the work of the metgrid program, like that of the ungrib program, is time-dependent, metgrid is run every time a new simulation is initialized.

Control over how each meteorological field is interpolated is provided by the METGRID.TBL file. The METGRID.TBL file provides one section for each field, and within a section, it is possible to specify options such as the interpolation methods to be used for the field, the field that acts as the mask for masked interpolations, and the grid staggering (e.g., U, V in ARW; H, V in NMM) to which a field is interpolated.

## **real Module**

The WRF model has two large classes of simulations that it is able to generate: those with an ideal initialization and those utilizing real data. The idealized simulations typically manufacture an initial condition file for the WRF model from an existing 1-D or 2-D sounding and assume a simplified analytic orography. The real-data cases usually require pre-processing from the WPS package, which provides each atmospheric and static field with fidelity appropriate to the chosen grid resolution for the model. The WRF model executable itself is not altered by choosing one initialization option over another (idealized vs. real), but the WRF model pre-processors (the real.exe and ideal.exe programs) are specifically built based upon a user’s selection. The real-data WRF cases are those that have the input data to the “real.exe” program provided by the WRF Preprocessing System (WPS). This data from the WPS was originally generated from a previously-run external analysis or forecast model. Here, real case was designed and implemented.

## **wrf Module**

This is the numerical weather prediction part of the modeling system. WRF can be used for a broad spectrum of theoretical and real-time studies, including applications of both predictive simulation and four-dimensional data assimilation to monsoons, hurricanes, and cyclones. On the smaller meso-beta and meso-gamma scales (2-200 km), WRF can be used for studies involving mesoscale convective systems, fronts, land-sea breezes, mountain-valley circulations, and urban heat islands. The WRF model is a fully compressible and non-hydrostatic model (with a run-time hydrostatic option). Its vertical coordinate is a terrain-following hydrostatic pressure coordinate. The grid staggering is the Arakawa C-grid. The model uses the Runge-Kutta 2nd and 3rd order time integration schemes, and 2nd to 6th order advection schemes in both the horizontal and vertical. It uses a time-split small step for acoustic and gravity-wave modes. The dynamics conserves scalar variables.

WRF is based on primitive physical equations of momentum, thermodynamics, and moisture. The state variables are temperature, specific humidity, grid-relative wind components, and pressure. Several model physics options in WRF are put together including radiation, convective parametrization, planetary boundary layer processes, surface layer processes and resolvable-scale microphysics schemes.

### **2.3.1.3 WRF-ARW Setup**

The modeling domain is built up according to synoptic systems having high impacts on most of Europe that involve Iceland low-pressure system around Iceland, Azores Low-pressure system around the Azores in the North Atlantic Ocean, Siberia High-pressure system and Basra Low-pressure system. It is defined between latitudes of 25-65 °N and longitudes of 20 °W- 50 °E that is covering continental Europe, North Africa in the south and Caspian Sea in the east (Figure 2.8). The Model has 30 km spatial resolution that is higher than continental US (CONUS-36 km) default mother domain resolution and also it has 35 vertical layers. The grid cell numbers in the modeling domain is defined for the south-north direction 159, for the west-east direction 191. ECMWF Era Interim reanalysis dataset (0.75°) that has higher spatial resolution than other datasets is used to create initial and boundary conditions of

the WRF model for the study period. MODIS-30s terrestrial data was used with 20 different land use category. The microphysics scheme is defined as WRF Single Moment 3-Class (Hong, Dudhia, & Shu-Hua Chen, 2004) in the model. The RRTM (Rapid Radiative Transfer Model) longwave radiation scheme (Mlawer, Taubman, Brown, Iacono, & Clough, 1997) and the Dudhia shortwave radiation scheme (Dudhia, 1989) are selected for the radiation schemes. Pleim-Xu scheme is applied to solve the surface physics. ACM2 (Pleim) (Pleim & Xiu, 1995) scheme is used for the planetary boundary layer physics and Kain-Fritsch scheme (Kain, 2004) is applied for cumulus parametrization.

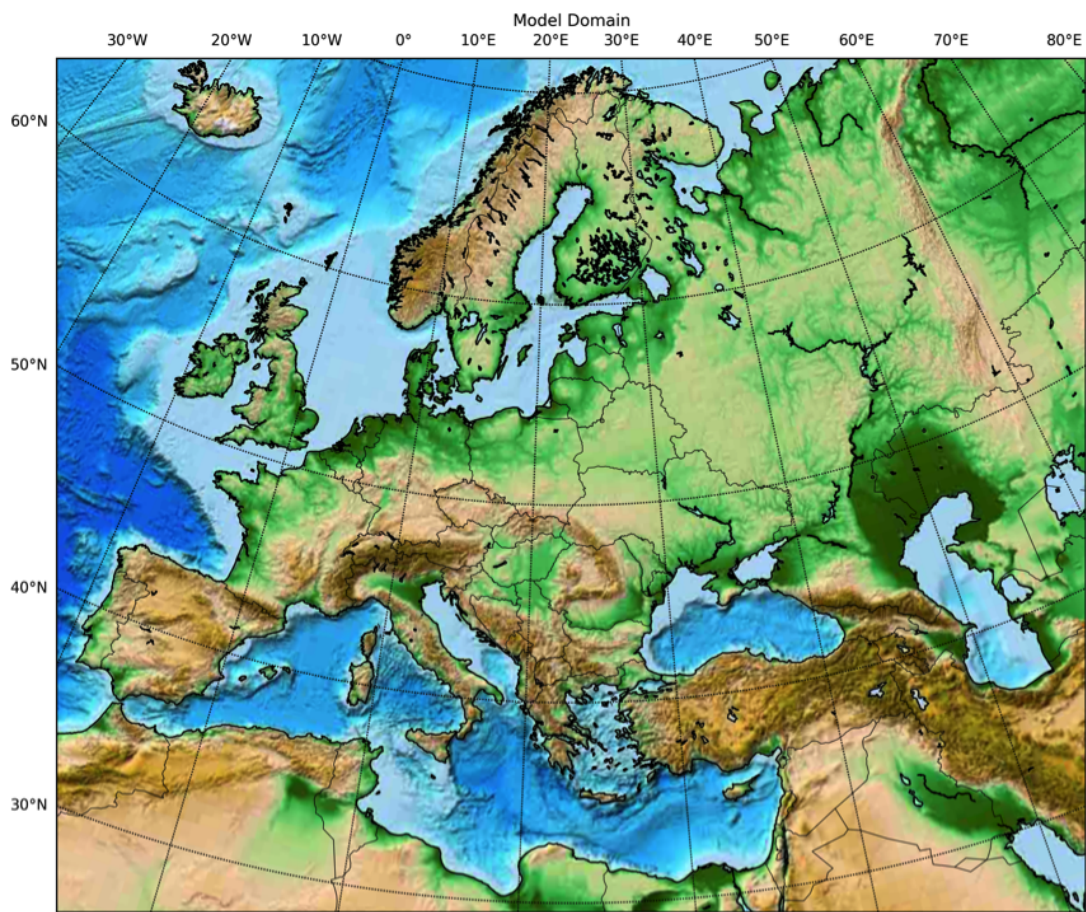


**Figure 2.8 :** WRF Modeling Domain - 30 km x 30 km spatial resolution

### 2.3.2 Emission Processing

Reliable emission inventory must be used in air quality modeling studies to create more accurate results. Emission inventory is a dataset that includes amounts of the emissions and their spatial and temporal distributions for air pollution sources. Emission inventories are basically established with bottom-up approach processing available

statistics on combustion, industrial activities and using appropriate emission factors. Basically, emission sources can be divided into four types which are anthropogenic, biogenic, fire and dust emission sources. These types of sources except dust emissions are used in this study. Because, in the case  $O_3$  and its effect are being investigated and dust emissions include only particulate matter that is not related to  $O_3$  pollution.

### **2.3.2.1 Anthropogenic Emissions**

Anthropogenic emissions sources have 3 subcategories which are area, point and mobile source. Area emissions sources are defined as immobile and distributed over a region air pollution sources. Calculations of area emission sources are made based on areal information. Commercial and residential heating, material storage, treatment, disposal, agriculture, constructions, gas stations and areal industrial production facilities are considered as area sources. Area sources are responsible for mostly particulate matter emissions. Point sources can be defined as the points in a specific area. Power plants, steel and metal industry, mining industry, chemical industry, cement industry and petroleum industry are considered as point sources. Mobile sources can be classified as highway and other vehicles that includes trains, boats, aircrafts, non-road vehicles etc. Highway vehicles are responsible for CO, HC,  $NO_x$  and PM emissions especially in the cities (Unal, Frey, & Rouphail, 2004).

Due to a number of gaps in country specific official inventories, global and regional emission inventories come up with advantages to use in modeling studies. TNO emission inventory based on 2009 (TNO2009) is used to prepare emission inputs for the air quality model in this study. It covers the regional Europe with 0.1 degree spatial resolution. Spatially distributed TNO2009 includes all emission source categorized by SNAP (Selected Nomenclature for Air Pollution) sectors. TNO2009 has 13 SNAP sectors, namely, Energy industries (S1), Non-industrial combustion (S2), Industry (combustion + processes) (S34), Extraction and distribution of fossil fuels (S5), Product use (S6), Road transport (S7, this has 5 subcategories), Non-road transport and other mobile sources (S8), Waste treatment (S9) and Agriculture (S10). Annual total emissions in the inventory are adjusted to the modeling domain by using intersection method. Additionally, TNO2009 does not cover North African and Middle Eastern Countries. Because of this, HTAP global emission inventory (based on 2010)



is used to cover these regions and it combined according to sectors with intersected TNO inventory.

The emission modeling process includes reading emission inventories and applying chemical speciation, temporal and spatial allocation, and control factors. For these purposes, DUMANv2.0 that is an emission-processing model is developed by Eurasia Institute of Earth Science, Istanbul Technical University. CB5 and AERO5 chemical and aerosol mechanisms are applied to the raw emissions in the model due to appropriate for European emission profiles.

#### **2.3.2.2 Biogenic Emissions**

Biogenic emissions (Biogenic Volatile Organic Compounds -BVOCs) are emitted from vegetation to the atmosphere. They are significantly important in the formation of secondary pollutants such as ozone and secondary organic aerosols. Global-Model of Natural Volatile Organic-Compound Emissions is developed by (Guenther et al., 1995) and they give the name of MEGAN. Along with developments in technology and measurement techniques, MEGAN is also developed and improved, especially having updated isoprene, terpene, and other VOC species. Latest version of MEGAN is version 2.10 , which is utilized in this study to provide biogenic emissions to our model run.

#### **2.3.2.3 Wildfire Emissions**

Biomass burning is a natural process in many ecosystems, but is greatly influenced by human activity and also by climate change. In many parts of the world, fire is used intentionally in agricultural practices.

Biomass burning plays a key role in public health and environmental issues. Fires contribute to the build-up of atmospheric carbon dioxide (CO<sub>2</sub>) and emit other greenhouse gases and are a major source of aerosols (in particular black carbon and organic carbon), carbon monoxide (CO), oxides of nitrogen (NO<sub>x</sub>) and other reactive trace gases, impacting local and regional air quality. The degree of human exposure depends on the fire location, amount of fuel burned, type of fire, and the atmospheric transport of and chemistry in the plume.

Emissions from open-vegetation burnings are increasingly recognized as an important parameter in atmospheric modeling, and their accurate description is important for specific regions and seasons as well as for specific episodes. Recent studies have demonstrated that open biomass-burning events, although episodic, may have important effects on the photochemistry in the eastern Mediterranean. Furthermore, the impact of biomass burning is expected to become more important in the southeastern Mediterranean according to future scenarios on climate change (Migliavacca et al., 2013).

Satellite remote sensing provides an automated means of locating and characterizing active fires. The fire size and their emissions in the atmosphere depend on the amount of material burned but also by natural climatic and orographic factors. For these reasons the emissions from fires are extremely variable and very difficult to estimate with low rate of uncertainty.

Different fire emission inventories were built based on the relationship between burned area, fuel load and combustion completeness and evaluating these variables on regional to global scale. One of these is the Global Fire Emissions Database (GFED3.1), that provide fire emissions calculations at a monthly temporal resolution and a  $0.5^\circ \times 0.5^\circ$  spatial resolution from 1997 to 2009, which is based on MODIS active fire data and global biogeochemical modeling.

The radiative component of the energy liberated by burning fuel can be measured by remote sensing, and spaceborne fire radiative energy (FRE) measures can potentially provide detailed information on the amount and rate of biomass consumption over large areas. In order to implement this approach, spaceborne sensors should have the capability to derive fire radiative power (FRP) estimates from subpixel fires using observations in just one or two spectral channels.

Quantifying emissions based on FRE eliminates the need to separately assess burned area, fuel loads, and combustion rates, and therefore removes a whole series of uncertainties due to our often rather limited knowledge of these variables. Observed FRP has been successfully used to calculate biomass combusted from wildfires using SEVIRI (Spinning Enhanced Visible and Infrared Imager) radiometer onboard the geostationary Meteosat-8 platform in Africa and MODIS data in both Africa and globe.

The Global Fire Assimilation System (GFASv1.0) calculates biomass burning emissions by assimilating Fire Radiative Power (FRP) observations from the MODIS instruments onboard the Terra and Aqua satellites. It corrects for gaps in the observations, which are mostly due to cloud cover, and filters spurious FRP observations of volcanoes, gas flares and other industrial activity. The combustion rate is subsequently calculated with land cover-specific conversion factors. Emission factors for 40 gas-phase and aerosol trace species have been compiled from a literature survey. The corresponding daily emissions have been calculated on a global  $0.5^\circ \times 0.5^\circ$  grid from 2003 to the present (Baldassarre et al., 2015).

### **2.3.3 Chemical Transport Model**

#### **2.3.3.1 The Community Multi-Scale Air Quality Model (CMAQ)**

USEPA has launched Models-3 Project to deal with modeling of atmosphere-land interaction, transformation and deposition. CMAQ model as a regional chemical transport model works for these purposes and it serves as multi-scale model compare to other air quality models (Ching and Byun, 1999). It is a three-dimensional Eulerian model. It simulates multiple pollutants such as ozone, particulate matter, other primarily pollutants, secondary organic aerosols etc. (CMAS, 2015). The CMAQ has basically five modules:

- Meteorology-Chemistry Interface Processor (MCIP)
- Photolysis Rate Processor (JPROC)
- Boundary Condition Processor (BCON)
- Initial Condition Processor (ICON)
- The CMAQ Chemistry - The Chemical Transport Model (CCTM) module.

Basic modeling framework starts with MCIP. MCIP converts the meteorological model's outputs to appropriate format of models-3. JPROC calculates clear sky photolysis rates according to constant tables. ICON and BCON creates chemical initial

and boundary conditions in vertical and horizontal for the domain. The framework of the model is shown in Figure 2.9.

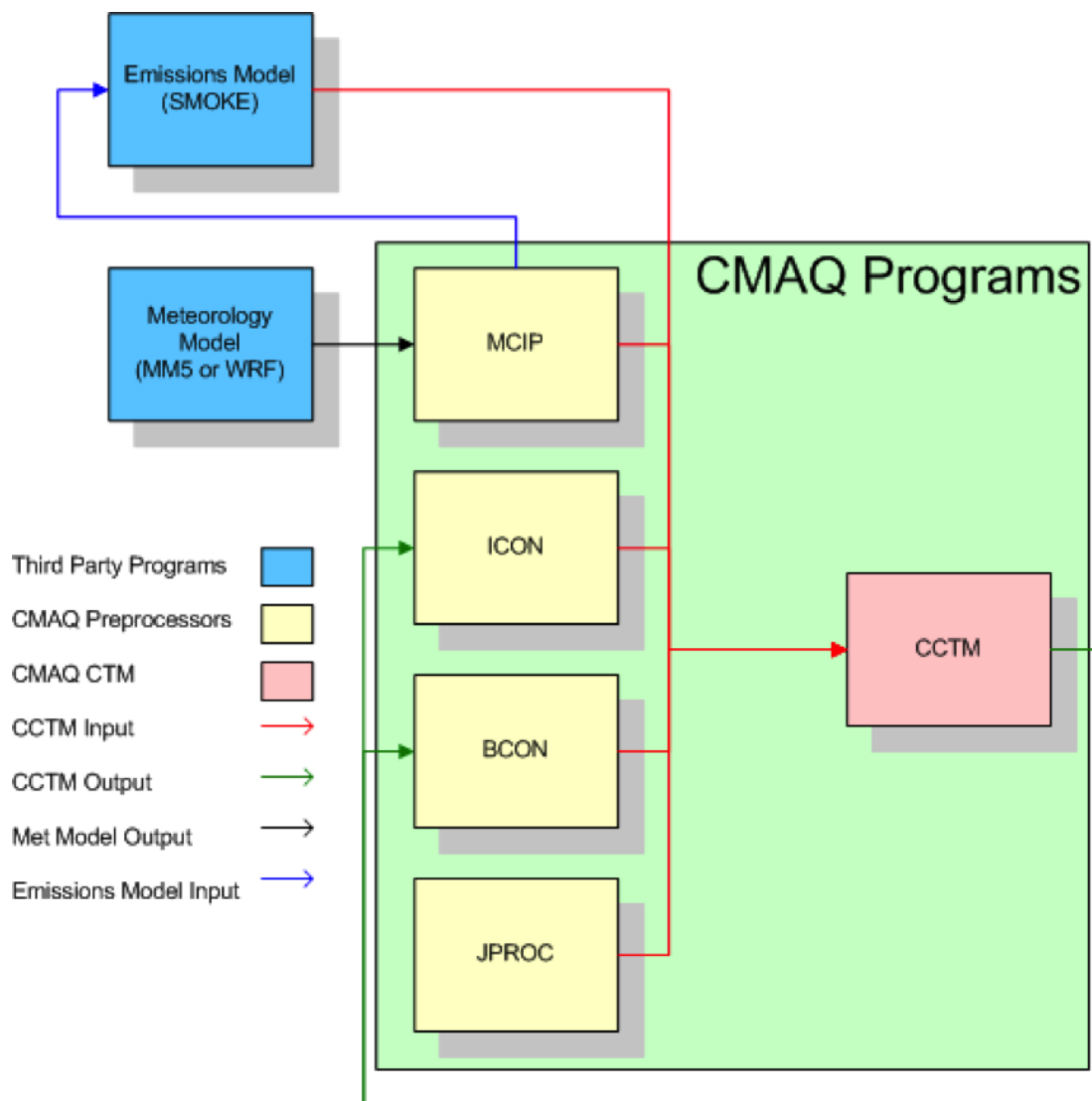


**Figure 2.9 : CMAQ Model Framework**

### 2.3.3.2 Major Modules of CMAQ

#### Photolysis Rate Preprocessor (JPROC)

JPROC calculates chemical-mechanism- specific clear-sky photolysis rates at fixed altitudes, hour angles, and latitude bands from tabulated absorption cross-section and quantum yield (CSQY) data. The only configuration option required for JPROC is the selection of the chemical mechanism to model. Output from JPROC is an ASCII lookup table of photolysis rates that the CCTM uses to calculate gas-phase chemical transformations and pollutant concentrations.

### **Initial Conditions Processor (ICON)**

ICON generates a gridded binary netCDF file of the chemical conditions in the modeling domain for the first hour of a simulation. It can generate these initial conditions from either an ASCII file of vertically resolved concentration profiles or from an existing CTM output file. If the ASCII profiles do not have the same vertical structure as the CTM configuration, ICON will interpolate the data to a vertical structure consistent with the CTM's. Using an existing CTM output file to generate initial conditions is applicable when extrapolating initial conditions from a coarse to a fine grid simulation, as may occur when setting up nested simulations. The configuration options for ICON include selecting the chemical mechanism to model, defining the horizontal and vertical grids, and choosing whether the initial conditions are generated from an ASCII profile or from an existing CCTM output file.

### **Boundary Conditions Processor (BCON)**

BCON generates a gridded binary netCDF file of the chemical conditions along the horizontal boundaries of the modeling domain. These boundary conditions can be either static or time-varying, and (as with ICON) can be generated from either an ASCII file of vertically resolved concentration profiles or from an existing CTM output file. BCON differs from ICON in that it can generate time-varying (i.e., dynamic) boundary conditions. Dynamic boundary conditions are typically extracted from CTM outputs from a coarse grid simulation for nested simulations or from a CTM simulation using a global-scale model. The file structure of the ASCII input profiles can also support the creation of dynamic boundary conditions, but generally these files are used for creating static data. The configuration options for BCON include selecting the chemical mechanism to model, defining the horizontal and vertical grids, and choosing whether the boundary conditions are generated from an ASCII profile or from an existing CTM output file.

### **Meteorology-Chemistry Interface Processor (MCIP)**

MCIP uses MM5 or WRF output files to create netCDF-based input meteorology for the emissions model and the CTM. MCIP prepares and diagnoses all meteorological fields that are required for the emissions model and the CTM. In addition, MCIP

is currently used to calculate the time- varying, species-dependent dry deposition velocities that are used in the CTM. MCIP can be used to uniformly trim cells off the boundary of the domain defined by the meteorological model, or to window in on a subset of that domain. MCIP can also decrease the vertical resolution of the meteorological data by “layer collapsing”, although this option should be used with caution as it can degrade the quality of the data if used incorrectly. Configuration options for MCIP include the time periods over which to extract data from the meteorological model output files, horizontal and vertical grid information, and selections for either passing through certain MM5-calculated variables unaltered or recalculating these variables within MCIP.

### **CMAQ Chemistry-Transport Model (CCTM)**

The CCTM integrates the output from all of the preprocessing programs, including the emissions and meteorology models, to simulate continuous atmospheric chemical conditions. The concentrations of relevant species can be captured for output at a user-definable frequency (typically hourly). The CCTM output files (some of which are “optional”) are all binary netCDF files of gridded and temporally resolved air pollutant information, such as gas and aerosol-phase species mixing ratios, hourly wet and dry deposition values, visibility metrics, and integral- averaged concentrations. The spatial and temporal extent of the CCTM output is dictated by the input meteorology. The science configuration is specific to each application of the model and can be adjusted to optimize model performance both computationally and in the numerical reproduction of observed air quality trends. Configuration options for the CCTM include the temporal coverage of the simulation, the chemical mechanism to model, the physics scheme to use for modeling pollutant transport, heterogeneous and aqueous chemistry options, plume-in-grid options, and diagnostic options (such as process analysis). The CCTM has the largest number of configuration options of all the CMAQ programs.

#### **2.3.3.3 Input Data and Chemical Mechanism**

CMAQ version 4.7, released in June 2010, is used in this study to investigate regional air quality. MCIP is prepared the meteorological fields that come from WRF model and 35 vertical layers used in WRF simulation are reduced to 24 layers for the

CMAQ simulation. JPROC is calculated the photolysis rates for study period. Initial and Boundary conditions is obtained from global simulations of ECMWF MACC Reanalysis project (spatial resolution 80-100km) and it is processed to change speciation according to our case. The dataset has 60 levels, from surface to 0.1 hPa. IC/BC are prepared by using this dataset as an input to CTM. The Carbon Bond-V (CB05) mechanism was used to model ozone, particulate matter, visibility, acid deposition and air toxic issues (Yardwood, Rao, Yocke, & Whitten, 2005). Global mass conserving scheme Yamo was used for vertical and horizontal advection. Vertical diffusion was represented by an updated version of Asymmetric Convective Method. Chemical kinetics was solved by using Euler backward approximation (EBI) that is based on nonlinear differential equations. AERO5 and ACM modules were used for aerosol and cloud simulation option, respectively (Foley et al., 2010).

### 2.3.4 Calculation of the Crop Production Loss and Economic Damages

In the literature, there are many field studies and different open-top chamber experiments conducted in different parts of the world with various crop types to evaluate the effects of ozone on agriculture (Heck, 1989; Krupa et al., 1998; Mills et al., 2007; Emberson et al., 2009). Two important projects: US National Crop Loss Assessment Network (NCLAN) studies (Heagle, 1989) and European Open-Top Chamber Program (EOTCP) were established in the 1980s and the beginning of the 1990s (Jager, Unsworth, De Temmerman, & Mathy, 1992). In this study, ozone exposure metrics applied in different regions of the world (AOT40, W126 and M7 Metric) were performed (Table 2.1). Expressions in table refer to: n is the number of hours in study period, i is the hourly index, Conc is the hourly ozone concentrations.

**Table 2.1** : Description of ozone exposure indices

Index	Equation	Unit
<b>AOT40</b>	$\sum_{i=1}^n [Conc_{ozone} - 30]_{i, for 08:00-19:59h and Conc \geq 40 ppb}$	ppb-h
<b>W126</b>	$\sum_{i=1}^n \left[ \frac{Conc_{ozone}}{1 + 4403xe^{-0.126xConc_{ozone}}} \right]_{i, for 08:00-19:59h}$	ppb-h
<b>M7</b>	$\frac{1}{n} \sum_{i=1}^n [Conc_{ozone}]_{i, for 08:00-19:59h}$	ppb-v

The AOT40 is an adopted metric in EU to evaluate accumulated ozone exposure over a threshold of 40 ppb for the daylight time (08:00-19.59h) during growing season. This method is currently in-use for regulation of air quality (Fuhrer, Skärby, & Ashmore,

1997). (Mills et al., 2007) made a review study in Europe and they have been obtained exposure-response function (Crop-Response function, CR) for different types of agricultural crops. W126 ozone exposure metric as secondary standards has been applied by the US EPA and many researchers. This metric is calculated by summing daylight-time (08:00-19.59h) hourly ozone concentrations (weighting comes from sigmoidal weight function) during growing season (USEPA, 1996). (USEPA, 1996) reported the CR- functions were obtained through experiments conducted. While sigmoidal function of the W126 metric is emphasizing peak values and exposure time of ozone concentrations, AOT40 metric gives equal weight to higher O<sub>3</sub> concentrations than 40 ppb (Tong et al., 2009). M7 metric described by (Tong et al., 2009) is the third metric selected for this study. This method is calculated by summing the 7h mean O<sub>3</sub> concentrations in daylight-time (09:00 – 15:59 h) during growing season.(Adams, Glyer, Johnson, & McCarl, 1989)) reported the exposure response functions of M7 for wheat. Differently from other metrics (AOT40 and W126), M7 index is calculated by giving equal weight to O<sub>3</sub> concentrations. Determined CR functions for all metrics were given in Table 2.2.

**Table 2.2** : Crop Exposure- Response (CR) functions for wheat used in the study to assess the Relative Yield Losses (RYL)

Exposure- Response (CR) Equations (RY) for each metric	References
$RY_{AOT40} = - 0.0161 \times AOT40 + 0.99$	Mills et al. (2007)
$RY_{W126} = \exp[- (W126 / 51.2)^{1.747}]$	Adopted by EPA (1996)
$RY_{M7} = \exp[- (M7/186)^{3.2}] / \exp[- (25/186)^{3.2}](\text{spring})$	Adams et al. (1989)

Despite there are more index to asses the risk of ozone to agriculture in the literature, These three methods are included in this study because they are considered to be mathematically superior aspects to the each other. In addition, when these three methods were examined in comparison, the analyses can give idea about the range of ozone-induced crop production loss and economic damage.

Firstly, ozone exposures were calculated with these three metrics mentioned above in detail. CR functions were applied by calculated ozone exposure for the each metrics and relative yield (RY) values were obtained from the CR functions. These values were scaled to RY is equal to 1 (Van Dingenen, 2009). Relative yield loss (RYL) with these values (RYL=1-RY) was calculated. Crop production loss (CPL) in each grid



cells was estimated applying Equation 1. CP shows the crop production in each grid cells. Additionally, The best way to calculate economical damage so is to compare the relative wheat losses of the countries and/or regions using consumer prices. However, as stated in (Avnery et al., 2011) actual price data information is insufficient, and hence, producer prices are used in the rest of the analysis. In particular, we use the FAO Wheat Producer Price Index that measures annual changes in selling prices received by farmers at the farm-gate or at the first point of sale. The economic losses (damages) are calculated using producer price (per ton) for 2009 multiplied by the national (or regional) wheat loss (i.e., CPL). Although the absolute figures are useful to see both the individual magnitude (i.e., the effect on a single country) and also the overall impact of losses (i.e., the effect on a region), a better approach will be normalizing the data. In other words, dividing the related loss by GDP enables easy comparisons across countries and indicates whether a national government proportionately loses more or less than the others. Therefore, loss calculated by AOT40, as well as that by W126 and M7, are divided by national  $GDP_{2009}$  levels at current market prices of each country.



### **3. RESULTS & DISCUSSION**

#### **3.1 Model Performance**

In this part of the study, the performance of the WRF/CMAQ modeling system was evaluated. O<sub>3</sub> observations were obtained from AirBase database for the period of 2009 growing season and simulated O<sub>3</sub> produced with WRF/CMAQ modeling system were used for this analysis. The performance was evaluated using Mean Normalized Bias (MNB). We have mapped the results of 1262 stations included in the performance analysis to evaluate the regional variation. There is no observational data for Russia, Belarus, Ukraine, Turkey, Georgia, Middle-East Countries and North African countries in Airbase, thus no conclusions for these countries. In spite of this, the observation network of the air quality monitoring stations in European Countries is enough to make the performance analysis.

Figure 2.1-a shows that mean ozone concentrations for each station over the growing season period in 2009. Southern and Central European countries have a tendency to have higher ozone levels. Mean ozone values were around 30 – 42 ppb over a wide area in Europe. Especially, stations close to Mediterranean Sea show the significant mean ozone concentrations (over than 45 ppb). The mean normalized bias (MNB, range -1 to 1) values were found higher where the topography is more complex. The MNB were calculated relatively high in Austria, Northern Italy and Romania where mean ozone values are higher than 35 ppb. The model overestimated over those regions due to topography. Although the MNB was negative in the UK and Northern Germany, the values were very low. The values of MNB in the rest of the stations were lower (Figure 3.1). The results of the WRF/CMAQ modeling system are very promising looking at the performance analyses in terms of MNB. In the overall performance analysis, MNE (range 0% to  $+\infty$ ) showed that model was not perfect in the Central Europe and partially Balkans. RMSE (ppb) showed that the accuracy was less than 20 ppb in the most part of Europe (Appendix D).

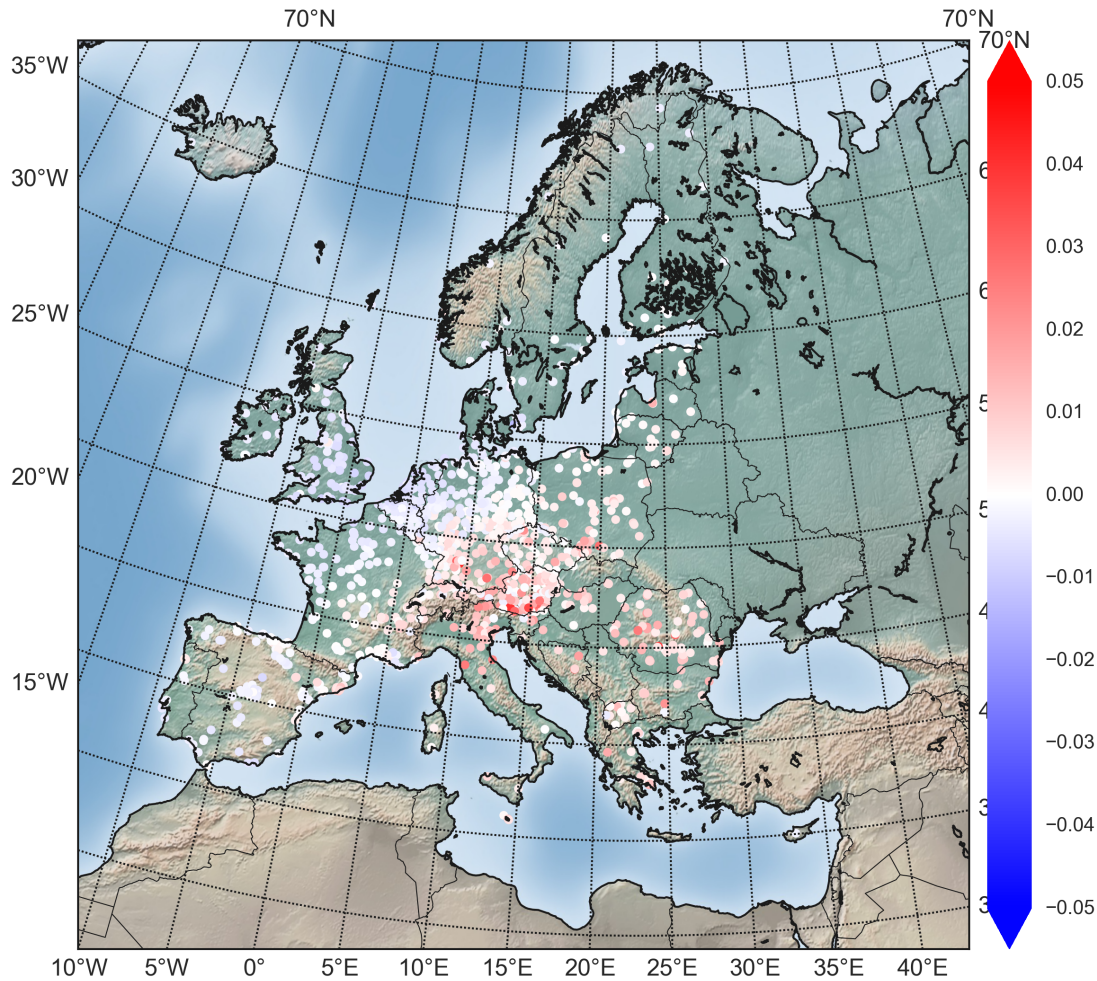


**Figure 3.1 :** CMAQ Model Performance- Mean Normalized Bias Results for Each Station in the AirBase

### 3.2 Crop Production Loss

Figure 3.2(a,c,e) demonstrates crop (wheat) production loss (ton) calculated by ozone observations using three different ozone vegetation exposure indices during growing season (May-July) in 2009. However, it was difficult to determine the damages via observational analysis due to lack of network coverage. Therefore, the same analysis was performed with the model outputs for the same period. When calculated crop production losses with observations and model outputs were compared, model caught high crop production losses (spatially) calculated with observations, except Northern Spain (Figure 3.2).

The significant wheat production loss can be found in all analysis. The production loss seems to be more in some countries, which have coasts to Mediterranean Sea than

other countries. AOT40 based calculation showed the loss was higher than 50.000 ton in each grid cell of Nile delta located in Egypt and Po valley located in Northern Italy. Additionally, the loss was calculated to be more than 50.000 ton in some grid cells along the coastlines of Croatia and Albania. Similarly, the higher production losses were found more than 35.000 per grid cell ton in Northwestern Turkey – is called Thrace – and along the coastline of Bulgaria. Central European countries such as Germany, Hungary, Czech Republic indicated that the loss was more than 20.000 ton per grid cell. Although France is one of the most important wheat producers, the loss per grid cell (less than 15.000 ton) was relatively lower than other countries (Figure 3.2-b).

Figure 3.2-d shows that the wheat production loss calculated using M7 index was considerably higher than 40.000 ton in each grid cell of the Po valley (Northern Italy), Nile Delta (Egypt), Crimea, Krasnodar Krai (the province of Russia that is located at south of Russia), Southern Romania, Bulgaria as well as Thrace (Northern Turkey). Also similar values were found in the region from Northern Anatolia to Central Anatolia. The loss was calculated more than 32.000 ton per grid cell around the Gulf of Issus (Southern Turkey and Western Syria). Similarly, Northern Tunisia showed that loss was higher 28.000 ton. After these regions, Central European countries (Hungary, Slovakia and Germany) and central France showed high wheat production loss that is more than 20.000 ton.

The analysis with W126 index indicated the same regions with AOT40 based calculations have high production loss. However, the amounts of losses were lower in W126 based method. The loss was determined to be more than 20.000 ton in each grid cell in Po Valley and Nile Delta. These values were the highest in the analysis made with W126 index. The loss was higher than 18.000 ton in each grid cell along the coastline of Croatia and Albania around the Adriatic Sea. Wheat production loss has been identified to be more than 6000 ton in Thrace (Northwestern Turkey). Central European countries and France indicated that the loss was 4000 ton per grid cell (Figure 3.2-f).

Total wheat production loss and their percentage losses (fractional loss) given in the Figure 3.3 and 3.4 were calculated for the countries in the modeling domain. The

calculation made with AOT40 metric based on country totals indicated that Russia has the highest loss (7.14 Mt), which is corresponding 11.6 percent loss. Russia has the highest wheat production because of the large area of wheat plantation. Secondly, the total production loss in Italy was calculated to be 5.08 Mt. This loss is to be 77 percent of the total production. Ukraine has the third most loss around 4.13 Mt (19%). Calculated wheat production losses in Turkey and Egypt were found 3.2 Mt (15%) and 3.15 Mt (36%), respectively. Although the amounts of the loss were close in both countries, the percentages of the loss were shown it is higher in Egypt. The losses in Germany and France were determined to be 2.7 Mt (11%) and 2.4 Mt (6.1%), respectively. France and Germany have the highest wheat production after Russia. The losses were calculated between 1 Mt and 1.4 Mt in Romania, Hungary, Poland, Bulgaria, Iran and Czech Republic. The percentage losses in these countries were around 30 percent except Poland that was around 13 percent. Even though United Kingdom and Denmark have high wheat production, the losses were calculated 0.02 Mt (0.17%) and 0.14 Mt (2.3%), respectively. The losses in UK and Denmark were found quite low. The highest percentage loss was found in Albania (88%) and Italy (77%). The percentage loss was determined 62% and 55% in Croatia and Slovenia, respectively. The lowest percentage loss was found in Northern and Western European countries (UK, Ireland, Netherlands, Belgium, Finland, Norway, Denmark, Sweden-less than 4%). The highest total wheat production losses (8.7 Mt) were seen in Eastern Europe (Montenegro, Macedonia, Moldova, Bulgaria, Serbia, Romania, Ukraine, Bosnia and Croatia). The losses were determined as 6.14 Mt and 7.22 Mt in Southern and Central Europe, respectively. However, the percentage losses drew attention to Southern Europe with the value of 47%. The percentage of loss was around 24% in Eastern Europe. The lowest total loss (0.65 Mt) and lowest percentage loss (2.2%) were found in the countries of Northern Europe (Baltic countries) (Figure 3.3-a, Figure 3.4-a).

The highest production loss was found in Italy (1.54 Mt) in the analysis made with W126 metric based calculation. Also Italy is the second country in terms of the percentage of loss with the value of 24%. Russia and Ukraine followed Italy with the values of 0.72 Mt 0.67 Mt wheat losses. Fourth highest loss was found in Turkey that was around 0.47 Mt corresponding to 3.4% loss. The loss in Germany (0.45 Mt)



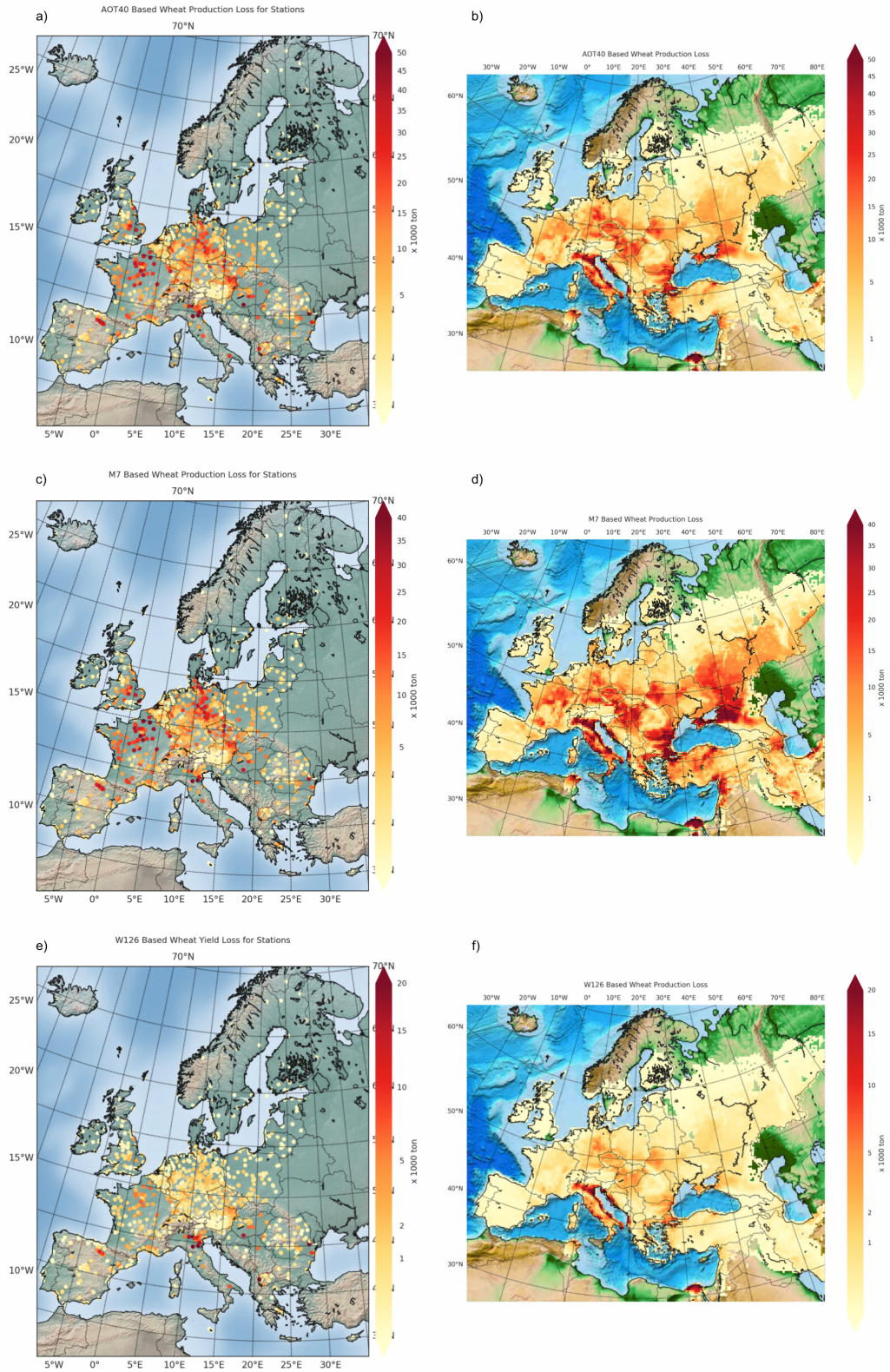


**Figure 3.2 :** Station based and model based CPL results for AOT40 metric (a,b), W126 (c,d) and M7 (e,f)

and Egypt (0.42 Mt) were close to Turkey's loss. The percentage of loss in Egypt was found 5%. Even though Hungary had 0.26 Mt production losses, the percentage of

loss was calculated 6%. The amount of loss was found 0.21 Mt and the percentage of it was calculated less than 1% in France. The losses Romania (0.23 Mt) and Poland (0.24 Mt) were close to each other, however, the percentages of losses were calculated lower, 4.4% and 2.4% respectively. The production and percentage loss in Bulgaria and Czech Republic were close to each other with the value of 0.19 Mt and 4.5%. Although Albania and Croatia had the losses 0.18 Mt and 0.09 Mt, the percentages of losses were relatively high values, 27% and 19% respectively. Greece as a southern European country showed that the loss calculated with W126 based analysis was 0.15 Mt and loss percentage was 8%. Minimum production loss and percentage loss were calculated in Northern and Western European countries. Especially, UK and Denmark as the highest wheat producer countries showed that the losses were quite low. The highest total wheat production losses (1.8 Mt) were found in Southern Europe due to high production loss in Italy. The total percentage loss of Southern Europe was determined as 13.3%. The losses were calculated as 1.4 Mt and 1.3 Mt in Eastern and Central Europe, respectively. The percentages of loss in those regions were less than 5%. The lowest production (0.07 Mt) and percentage loss (0.24%) was found in Northern Europe (Figure 3.3-b, Figure 3.4-b).

The catastrophic production loss calculated using M7 metric has been estimated in Russia (17.3 Mt). This was also the highest predicted production loss value in all analysis. Nevertheless, Russia's percentage of loss (28%) was lower than many other countries. Turkey and Ukraine where the percentage of losses were around 30% followed Russia in terms of the production loss with the value of 6.8 Mt and 6.65 Mt, respectively. Although Italy had 6.45 Mt production loss, the percentage of loss was calculated around 98% that is the highest value and the one of the significant results in the study. Egypt had the fifth highest production loss in the study with the value of 5.54 Mt. The losses in France and Germany were calculated to be 3.47 Mt and 2.45 Mt, respectively. The percentages of the losses in both countries were determined around 9%. Additionally, Losses in Germany and Romaine (2.26 Mt) were close to each other, however, the percentage of loss in Romania was higher 43%. The losses were calculated between 1 Mt and 1.5 Mt in Bulgaria, Hungary, Poland, Greece, Syria and Iran. The percentages of the losses were determined to be around 49%, except in Poland (12%) similar to AOT40 method outcomes. Czech Republic as a Central



European country indicated the loss was around 0.9 Mt and its percentage was 20%. Denmark and Lithuania showed the similar results for the loss that were around 0.2 Mt corresponding to low percentages of losses, 9% and 3%. Surprisingly, even though United Kingdom has the highest production in wheat, the loss was calculated quite low that was around 0.12 Mt and its percentage was 0.85%. As mentioned before, Italy and Albania (0.31Mt) showed that the highest losses in terms of percentage were with 98% and 95%, respectively. These results were followed by Croatia, Egypt, Israel, Slovenia, Greece, Bulgaria and Montenegro with the value of percentage of losses that was more than 50%.

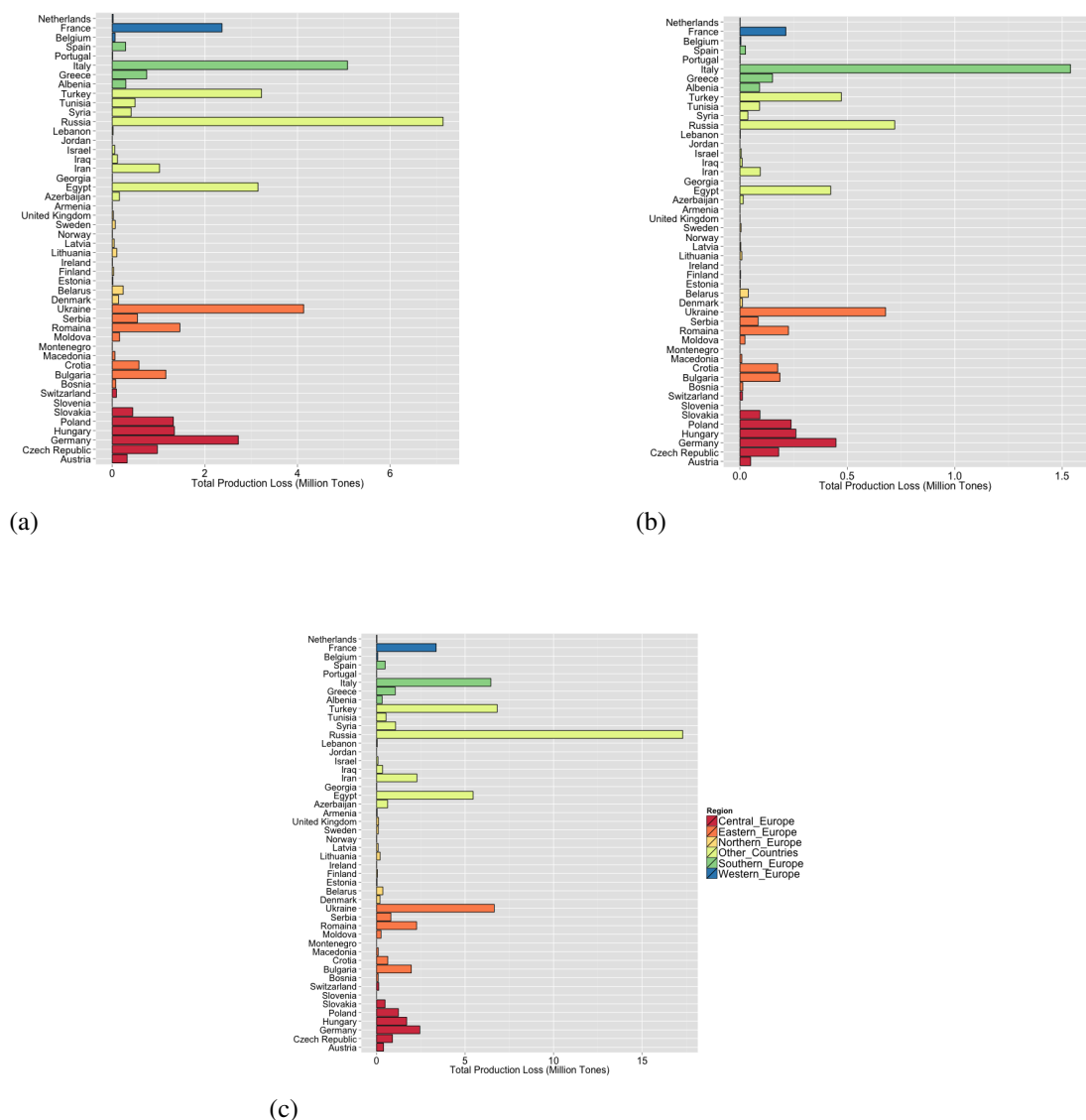
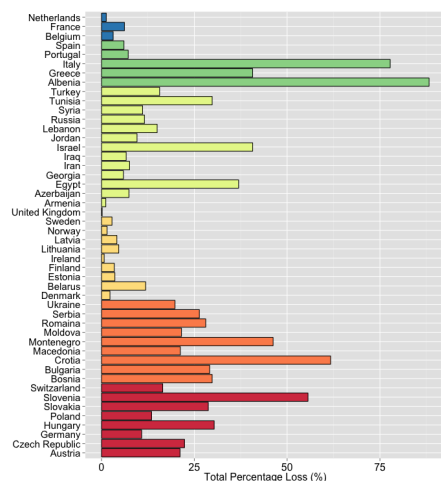
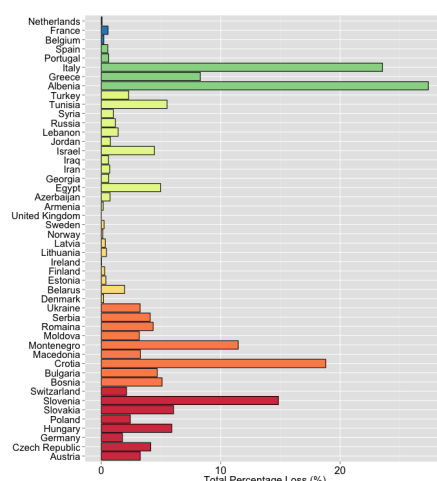


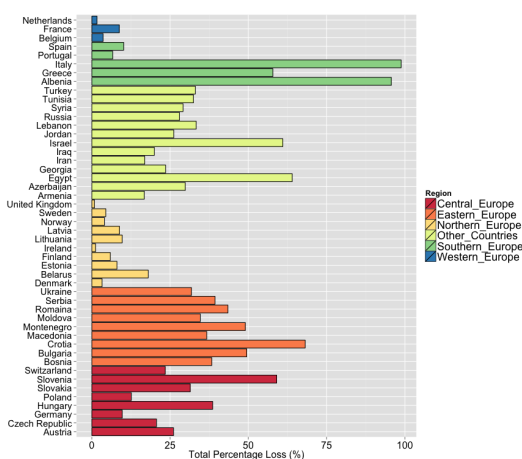
**Figure 3.3 :** Total production loss in the each country for AOT40 (a), W126 (b) and M7 (c)



(a)



(b)



(c)

**Figure 3.4 :** Total percentage (fractional) loss in the each country for AOT40 (a), W126 (b) and M7 (c)

The lowest percentage loss was found in Northern and Western European countries. The highest total wheat production losses (12.78 Mt) were seen in Eastern Europe. The losses were calculated as 8.3 Mt and 7.3 Mt in Southern and Central Europe, respectively. Although, the highest loss was found in Eastern Europe (37%), the highest percentage loss was calculated for Southern Europe with the value of 61%. The lowest total loss (0.65 Mt) and lowest percentage loss (2.2%) were found in the countries of Northern Europe (Baltic countries) (Figure 3.3-c, Figure 3.4-c).

Although, the W126 index and AOT40 index were pointing same regions for the higher production loss, the amount of the production loss were found lower in W126 metric based method due to weighting of the ozone concentrations in the function of W126. In addition to this, M7 metric based calculations indicated that the highest loss can be

happen in case of high ozone exposure during the limited daylight time. Therefore, it showed the highest loss in the all analysis.

### **3.3 Economic Damages**

This section evaluates the economic terms of wheat losses. The best way to do so is to compare the relative wheat losses of the countries and/or regions using consumer prices. However, as stated in Avnery et al (2011) actual price data information is insufficient, and hence, producer prices are used in the rest of the analysis. In particular, we use the FAO Wheat Producer Price Index that measures annual changes in selling prices received by farmers at the farm-gate or at the first point of sale. The economic losses (damages) are calculated using producer price (per ton) for 2009 multiplied by the national (or regional) wheat loss (i.e., CPL).

Based on AOT40 model, the highest economic loss occurred in Italy (\$1.29 Billion USD<sub>2009</sub>) followed by Turkey (\$1.06 Billion), Russia (\$0.96 Billion) and Egypt (\$0.92 Billion). These four countries account for more than half of the total loss in monetary terms in the entire region studied (Figure 3.5-a). Although the absolute figures are useful to see both the individual magnitude (i.e., the effect on a single country) and also the overall impact of losses (i.e., the effect on a region), a better approach will be normalizing the data. In other words, dividing the related loss by GDP enables easy comparisons across countries and indicates whether a national government proportionately loses more or less than the others. Therefore, loss calculated by AOT40, as well as that by W126 and M7, are divided by national GDP<sub>2009</sub> levels at current market prices of each country. In fact, the ranking calculated with the AOT40 model changes immediately as can be seen from Figure 3.6. Albania loses the most as a percentage of GDP with 6,68‰, followed by Egypt (4,84‰), Tunisia (3,61‰), Ukraine (3,58‰), and Bulgaria (3,35‰), whereas Italy (0,58‰) comes only 20th.

The analysis performed with W126 metric showed almost the same ranking results if not the numbers as above: the greatest economic loss was in Italy (\$0.39 Billion) followed by Turkey (\$0.16 Billion), Egypt (\$0.12 Billion) and Russia (\$0.1 Billion). Once again, more than half of the total loss in the studied region belongs to these four countries (around 57%) (Figure 3.5-b). The total loss is worth \$1.34 Billion,

**Table 3.1 : Regional calculated total economic loss (\$ Billion)**

Regions	AOT40		W126		M7	
	EL	EL/GDP (‰)	EL	EL/GDP (‰)	EL	EL/GDP (‰)
Northern Europe	0.10	0.002	0.01	0.0003	0.18	0.005
Western Europe	0.38	0.009	0.03	0.001	0.54	0.013
Eastern Europe	1.03	0.215	0.18	0.037	1.60	0.334
Southern Europe	1.61	0.038	0.46	0.011	2.08	0.049
Central Europe	1.12	0.021	0.20	0.004	1.14	0.022
Other Countries	3.70	0.090	0.46	0.011	7.87	0.192
European Countries	4.24	0.025	0.88	0.050	5.54	0.033

which makes almost one-fifth of the loss (17%) measured by AOT40. When it comes to EL/GDP based ranking, W126 leads no different than AOT40: Albania (2,07‰), followed by Tunisia (0,66‰), Egypt (0,65‰), Ukraine (0,58‰), and Bulgaria (0,53‰), whereas Italy (0,17‰) comes only 10th.

Finally, it is Russia that is projected to experience the highest loss with the M7 model. In fact, this is the highest single country loss calculated independent of the metric model. While Russia's loss amounts to \$2.33 Billion, loss of Turkey does not fall far, that is, \$2.24 Billion. These two are followed by Italy (\$1.64 Billion), followed by Egypt (\$1.59 Billion) and Iran (\$0.71 Billion). The losses of the top five above accounts for 64% of the total monetary loss calculated by M7 (Figure 3.5-c). However, when the data is normalized, it is Egypt at the top with 8,4‰. Albania (7,24‰), Ukraine (5,76‰), Bulgaria (5,69‰) and Moldova (4,05‰) follow. One should note that in all the models five countries with the lowest EL/GDP are always the same (though not necessarily in the same order): United Kingdom (sixth biggest producer in the region studied), Ireland, Netherlands, Norway and Slovenia.

Economic damages due to ozone induced wheat production losses in EU countries is estimated 4.24 Billion USD for AOT40 metric based calculation, 5.54 Billion USD for M7 metric based calculation and 0.88 Billion USD for the W126 model. This damage in Non-EU countries is calculated 3.7 Billion USD for AOT40 metric method. M7 and W126 indicates that the economic losses were 7.87 Billion USD and 0.46 Billion USD, respectively (Table 3.1).

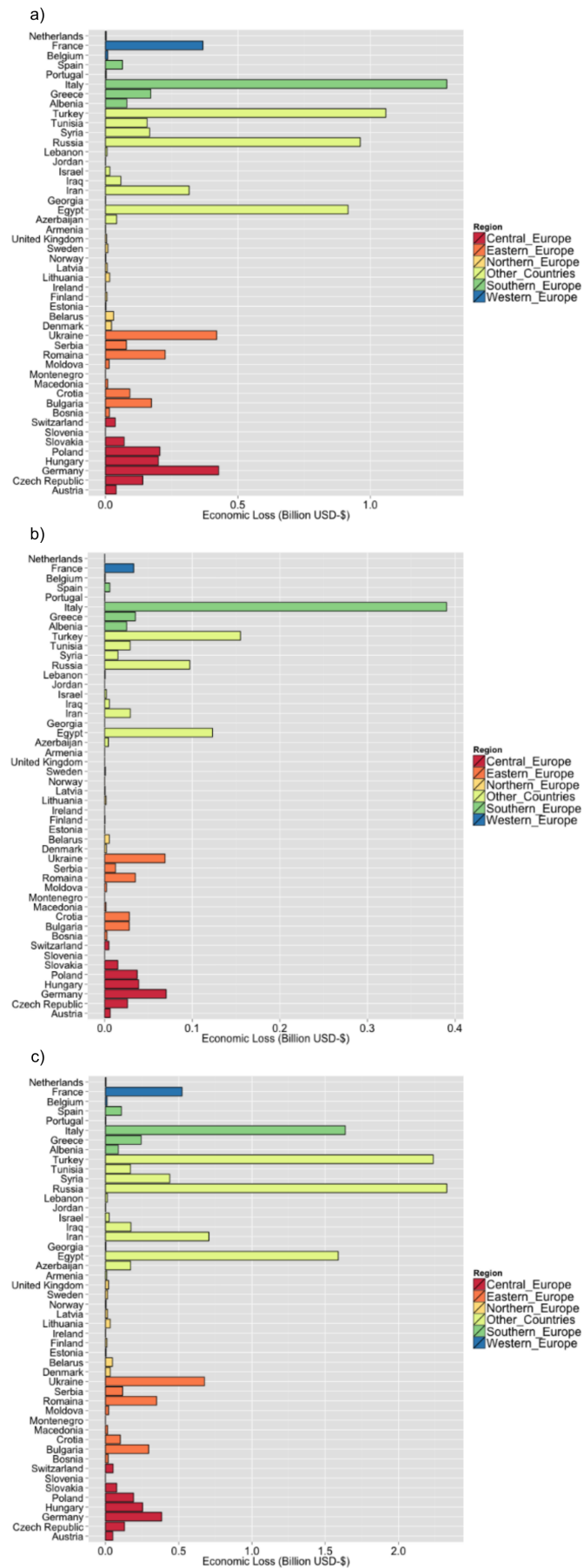


**Figure 3.5 :** Total Economic loss in the each country studied for AOT40 (a), W126 (b) and M7 (c)

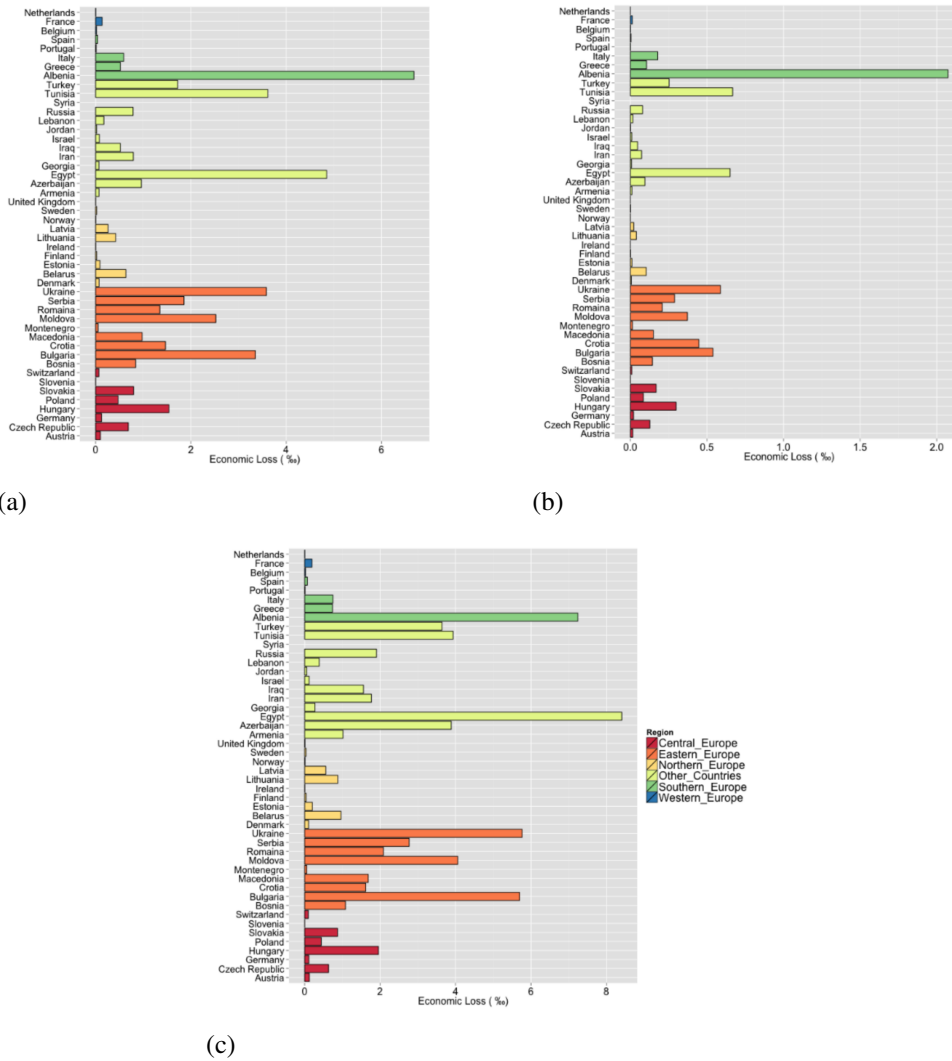


**Figure 3.6 :** Economic loss GDP in the each country studied for AOT40 (a), W126 (b) and M7 (c)

When European countries' economic losses are examined by regional basis, with the AOT40 method the greatest damage occurs in Southern Europe (\$1.61 Billion). In addition, economic losses in Central Europe (\$1.12 Billion) and Eastern Europe (\$1.03 Billion) are very close. The lowest economic damage occurs in Northern Europe (\$0.1 Billion). Southern Europe faces the highest economic loss (\$0.46 Billion) in the analysis applied W126 metric. The damages in Eastern EU and Central EU are estimated as 0.18 and 0.20 Billion USD, respectively. The minimum damage is found again in Northern Europe, which is 0.01 Billion USD. Additionally, M7 method indicates that Southern Europe (\$ 2.08 Billion) has the greatest economic loss. It is estimated 1.60 Billion USD in Eastern Europe. It is higher in Central Europe (1.14 Billion USD) than Western and Northern Europe.

Although the above discussion gives an insight about the absolute values of dollar losses regionally, it does not help much comparison-wise. Once again, normalizing with the help of GDP, it is straightforward from Table 3.1 that the highest damage occurs in Eastern Europe followed by the Southern Europe for all the models run. Similarly, it hurts more the Non-EU Countries than it hurts the EU Countries.

Three alternative methods (AOT40, W126 and M7) are used to analyze the wheat losses of 48 countries. The total USD loss is found to range from \$1.33 Billion (W126), to \$7.94 Billion (AOT40) and finally to \$13.4 Billion (M7). Betting on the worst-case scenario leads to a loss of \$13.4 Billion. It is worth 41.3% of the Ethiopian GDP<sub>2009</sub>.





#### 4. CONCLUSION

There is an increasing trend in ozone and its precursors emitted from anthropogenic sources. Ozone levels was 5 – 15 ppb in the mid-19<sup>th</sup> century, however, last three decades, it increased to 11- 46 ppb. Experimental and observational studies showed that elevated ozone might affect plants' life functions such as photosynthesis and transpiration throughout damaging the substomal apoplast, cell membranes and walls. However, due to transboundary transport and complex nature of formation of ozone, as a global problem, threatens not only vegetation, but also human health and food security. These issues are important for Europe, because 10% of the world population is living in Europe. In addition, wheat production in between 1996 – 2014 in Europe constitutes 21 % (133.9 Mt) of world's wheat production. Additionally, Europe is the place where the industrialization is relatively high which resulting in more tropospheric O<sub>3</sub> production and variability. However, there are not many studies focus on the impact of ozone on agriculture in Europe. This is the first study evaluating of the impact of ozone on agriculture and its economic damage in Europe via regional chemistry model CMAQ. Wheat production loss was calculated with 3 different ozone vegetation exposure indices for growing season of the year 2009 and then these indices gave a range between minimum and maximum loss in Europe. Even though, there is no exact method to figure out the crop loss due to ozone, providing a range is important to understand the variability of crop loss.

Three case showed the similar results in terms of ranking total crop losses in countries. When results for each country are evaluated individually, Russia, Italy, Turkey, Ukraine, Egypt, France and Germany showed mostly maximum crop loss. The minimum of the maximum crop loss was in France with the value of 2.4 Mt, the maximum crop loss was found in Russia (7.14 Mt) for the AOT40 based method. Similar results were found for W126 based method. The minimum of the maximum crop loss was found in France; again, with the value of 0.21 Mt and maximum crop loss in this method was in Italy (1.54 Mt). Additionally, In M7 based method, the minimum

of the maximum crop loss was found in Germany (2.45 Mt), and the maximum loss was in Russia with the value of 17.3 Mt. This was also the highest predicted crop production loss in all three analyses in the study. In regional basis analysis, the wheat production loss was found 6.14 Mt and 7.22 Mt in Southern and Central Europe, respectively, as a maximum loss in AOT40 based method. The lowest loss was estimated to be in Northern Europe (0.65 Mt). The maximum loss in W126 based method was in Southern Europe with the value of 1.8 Mt. Eastern and Central Europe followed with values of 1.4 Mt and 1.3 Mt. Again, Northern Europe had the lowest loss in the W126 based analysis. In M7 based method, the maximum loss was determined in Eastern Europe with the value of 12.78 Mt that was the highest estimated loss in all analysis. Southern and Central Europe followed Eastern Europe with 8.3 Mt and 7.3 Mt, respectively. Although, the W126 index and AOT40 index were pointing same regions for the higher production loss, the amount of the production loss were found lower in W126 metric based method due to weighting of the ozone concentrations in the function of W126. In addition to this, M7 metric based calculations indicated that the highest loss can be happen in case of high ozone exposure during the limited daylight time. Therefore, it showed the highest loss in the all analysis.

In percentage loss analysis, the maximum loss was found to be in Southern Europe (47% for AOT40, 13% W126 and 61% for M7) in all methods. After Southern Europe, Eastern Europe had the second highest loss in terms of percentage (24 % for AOT40, <5% for W126 and 37% for M7). Southern Europe mostly showed relatively high ozone levels in the study. This may be the reason of high percentage loss was found in there. In terms of amount of loss (production loss), maximum loss was in Eastern Europe. This may be because of transportation of ozone precursors from Northern and Western European countries to Eastern countries. That may cause an increase in ozone levels around Eastern Europe region. Also, low crop loss in Northern and Western Europe can support these interpretations.

Besides, based on AOT40 model, the highest economic loss occurred in Italy (\$ 1.29 Billion) followed by Turkey (\$1.06 Billion), Russia (\$0.96 Billion) and Egypt (\$0.92 Billion). These four countries account for more than half of the total loss in monetary terms in the entire region studied. The analysis performed with W126 metric showed almost the same ranking results if not the numbers as above: the greatest economic

loss was in Italy (\$0.39) followed by Turkey (\$0.16 Billion), Egypt (\$0.12 Billion) and Russia (\$0.1 Billion). Once again, more than half of the total loss in the studied region belongs to these four countries (around 57%). Finally, it is Russia that is projected to experience the highest loss with the M7 model. In fact, this is the highest single country loss calculated independent of the metric model. While Russia's loss amounts to \$2.33 Billion, loss of Turkey does not fall far, that is, \$2.24 Billion. These two are followed by Italy (\$1.64 Billion) and Egypt (\$1.59 Billion). In regional basis analysis, the maximum losses were calculated with M7 method for Southern (\$2.08 Billion) and Eastern Europe (\$1.60 Billion). Betting on the worst-case scenario leads to a loss of \$13.4 Billion. It is worth 41.3% of the Ethiopian GDP<sub>2009</sub>.



## REFERENCES

- Adams, R., Glyer, J. D., Johnson, S. L., & McCarl, B. A.** (1989). A reassessment of the economic effects of ozone on u.s. agriculture. *Journal of the Air Pollution Control Association-JAPCA*, 39(7), 960-968. doi: 10
- Arunachalam, S., Wang, B., Davis, N., Baek, B., & Jonathan, J. I.** (2011). Effect of chemistry-transport model scale and resolution on population exposure to pm2.5 from aircraft emissions during landing and takeoff. *Atmospheric Environment*, 45, 3294-3300.
- Avnery, S., Mauzerall, D. L., Liu, J., & Horowitz, L. W.** (2011). Global crop yield reductions due to surface ozone exposure: 1. year 2000 crop production losses and economic damage. *Atmospheric Environment*, 45, 2284 - 2296.
- Baldassarre, G., Pozzoli, L., Schmidt, C. C., Unal, A., Kindap, T., Menzel, W. P., ... Kaiser, J. W.** (2015). Using seviri fire observations to drive smoke plumes in the cmaq air quality model: a case study over antalya in 2008. *Atmos. Chem. Phys.*, 15, 8539-8558. doi: 10
- Bozo, L., & Weidinger, T.** (1995). Tropospheric ozone measurements over hungary in the 19th century. *Abio*, 23(2), 129-130.
- Cartalis, C., & Varotsos, C.** (1994). Surface ozone in athens, greece, at the beginning and end of the twentieth century. *Atmospheric Environment*, 28(1), 3-8.
- CMAS.** (2015). *Cmas model documentation* (Tech. Rep.). Retrieved from <https://www.cmascenter.org>
- Cohan, D., Hu, Y., & Russell, A.** (2006). Dependence of ozone sensitivity analysis on grid resolution. *Atmospheric Environment*, 40, 126-135.
- Cooper, O. R., Parrish, D. D., Stohl, A., Trainer, M., Nedelec, P., Thouret, V., ... Avery, M. A.** (2010). Increasing springtime ozone mixing ratios in the free troposphere over western north america. *Nature*, 463(1), 344-348. doi: 10.1038/nature08708
- Crutzen, P., Lawrence, M., & Pöschl, U.** (1999). On the background photochemistry of tropospheric ozone. *Tellus A: Dynamic Meteorology and Oceanography*, 51, 123-146.
- Debaje, S.** (2014). Estimated crop yield losses due to surface ozone exposure and economic damage in india. *Environmental Science and Pollution Research*, 21, 7329-7338.
- Dudhia, J.** (1989). Numerical study of convection observed during the winter monsoon experiment using a mesoscale two-dimensional model. *Journal of Atmospheric Science*, 46, 3077-3107.
- Emberson, L., Büker, P., Ashmore, M., Mills, G., Jackson, L., Agrawal, M., ... Wahid, A.** (2009). A comparison of north american and asian exposure-response data for ozone effects on crop yields. *Atmospheric Environment*, 43(12), 1945-1953.

- European Environment Agency (EEA).** (2013). *Airbase - the european air quality database*. Retrieved 26.07.2015, from <http://www.eea.europa.eu/data-and-maps/data/airbase-the-european-air-quality-database-8>
- Fishman, J., Watson, C. E., Larsen, J. C., & Logan, J. A.** (1990). Distribution of tropospheric ozone determined from satellite data. *Journal of Geophysical Research*, 95, 3599–3617.
- Foley, K. M., Roselle, S. J., Appel, K. W., Bhawe, P. V., Pleim, J. E., Otte, T. L., ... Bash, J. O.** (2010). Incremental testing of the community multiscale air quality (cmaq) modeling system version 4.7. *Geoscience Model Development*, 3, 126–135. doi: 10.5194/gmd-3-205-2010
- Food and Agriculture Organizations (FAO).** (2016). *Faostat*. Retrieved 21.11.2015, from <http://faostat.fao.org/>
- Fuhrer, J., Skärby, L., & Ashmore, M.** (1997). Critical levels for ozone effects on vegetation in europe. *Environmental Pollution*, 97(1-2), 91-106. doi: 10
- Ghude, S., Jena, C., Chate, D., Beig, G., Pfister, G., Kumar, R., & Ramanathan, V.** (2014). Reductions in india's crop yield due to ozone. *Geophysical Research Letters*, 41, 5685-5691. doi: 10.1002/2014GL060930
- Guenther, A., Hewitt, C. N., Erickson, D., Fall, R., Geron, C., Graedel, T., ... Zimmerman, P. A.** (1995). Global model of natural volatile organic-compound emissions. *Journal of Geophysical Research: Atmosphere*, 100(D5), 8873–8892.
- Heagle, A.** (1989). Ozone and crop yield. *Annual Review of Phytopathology*, 27, 397-423.
- Heck, W.** (1989). *Assessment of crop losses from air pollutants in the united states: Air pollution's toll on forests and crops*. Yale University Press, New Haven.
- Heck, W., Adams, R., Cure, W., A.S., H., H.E., H., Kohut, R., ... Taylor, O.** (1983). A reassessment of crop loss from ozone. *Environmental Sci. Technol.*, 17(12), 572A–581A.
- Hollaway, M. J., Arnold, S. R., Challinor, A. J., & Emberson, L. D.** (2012). Intercontinental trans-boundary contributions to ozone-induced crop yield losses in the northern hemisphere. *Biogeosciences*, 9, 271–292.
- Hong, S., Dudhia, J., & Shu-Hua Chen, S.** (2004). A revised approach to ice microphysical processes for the bulk parameterization of clouds and precipitation. *Monthly Weather Review*, 132, 103–120.
- Hunova, I., Livorova, H., & J., O.** (2003, February). Potential ambient ozone impacts on ecosystems in the czech republic as indicated by exposure index aot40. *Ecological Indicators*, 3, 35-47.
- Jager, H., Unsworth, M., De Temmerman, L., & Mathy, P.** (1992). Effects of air pollutants on agricultural crops in europe, results of the european open-top chambers project. *Air Pollution Research*, 46.
- Jen, M.** (2008). Trends in ozone concentration distributions in the uk since 1990: Local, regional and global influences. *Atmospheric Environment*, 42, 5434–5445.
- Kain, J.** (2004). The kain–fritsch convective parameterization: An update. *Journal of Applied Meteorology*, 43, 170-181.
- Krupa, S., Nosal, M., & Legge, A.** (1998). A numerical analysis of the combined open-top chamber data from the usa and europe on ambient ozone and negative crop responses. *Environmental Pollution*, 101, 157-160.

- Lamarque, J.-F., Bond, T. C., Eyring, V., Granier, C., Heil, A., Klimont, Z., ... van Vuuren, D. P.** (2010). Historical (1850–2000) gridded anthropogenic and biomass burning emissions of reactive gases and aerosols: methodology and application. *Atmospheric Chemistry and Physics*, 10, 7017–7039. doi: 10.5194/acp-10-7017-2010
- Logan, J.** (1999). An analysis of ozonesonde data for the troposphere: recommendations for testing 3-d models and development of a gridded climatology for tropospheric ozone. *Journal of Geophysical Research*, 104, 16115–16149.
- Logan, J. A., Staehelin, J., Megretskaia, I. A., Cammas, J.-P., Thouret, V., Claude, H., ... R., D.** (2012). Changes in ozone over europe: Analysis of ozone measurements from sondes, regular aircraft (mozaic) and alpine surface sites. *Journal of Geophysical Research*, 117(D09301).
- Malley, C., Heal, M., & Mills, C., G. and Braban.** (2015). Trends and drivers of ozone human health and vegetation impact metrics from uk emep supersite measurements 1990-2013. *Atmospheric Chemistry and Physics*, 15, 4025-4042.
- Migliavacca, M., Dosio, A., Camia, A., Hobourg, R., Houston-Durrant, T., Kaiser, J. W., ... Cescatti, A.** (2013). Modeling biomass burning and related carbon emissions during the 21st century in europe. *Journal of Geophysical Research: Biogeo.*, 118, 1732– 1747.
- Mills, G., Buse, A., Gimeno, B., Bermejo, V., Holland, M., Emberson, L., & Pleijel, H.** (2007). A synthesis of aot40-based response functions and critical levels of ozone for agricultural and horticultural crops. *Atmospheric Environment*, 41(12), 2630-2643.
- Mlawer, E. J., Taubman, S. J., Brown, P. D., Iacono, M. J., & Clough, S. A.** (1997). Radiative transfer for inhomogeneous atmospheres: Rrtm, a validated correlated-k model for the longwave. *Journal of Geophysical Research*, 102, 16663–16682.
- Monfreda, C., Ramankutty, N., & Foley, J.** (2008). Farming the planet: 2. geographic distribution of crop areas, yields, physiological types, and net primary production in the year 2000. *Global Biogeochemical Cycles*, 22(GB1022). doi: 10.1029/2007GB002947
- Morgan, P., Mies, B. G., T.A. and, Nelson, R., & Long, S.** (2006). Season-long elevation of ozone concentration to projected 2050 levels under fully open-air conditions substantially decreases the growth and production of soybean. *New Phytol*, 170, 333–343.
- Oltmans, S. J., Lefohn, A. S., Harris, J. M., Galbally, I., Scheel, H. E., Bodeker, G., ... Cuevas, E.** (2006). Long-term changes in tropospheric ozone. *Atmospheric Environment*, 40, 3156–3173. doi: 10.1016/j.atmosenv.2006.01.029
- Oltmans, S. J., Lefohn, A. S., Shadwick, D., Harris, J. M., Scheel, H. E., Galbally, I., ... Kawasato, T.** (2013). Recent tropospheric ozone changes - a pattern dominated by slow or no growth. *Atmospheric Environment*, 67, 331–351. doi: 10.1016/j.atmosenv.2012.10.057
- Parrish, D. D., Law, K. S., Staehelin, J., Derwent, R., Cooper, O. R., Tanimoto, H., ... Chan, E.** (2012). Long-term changes in lower tropospheric baseline ozone concentrations at northern mid-latitudes. *Atmospheric Chemistry and Physics*, 12(D09301), 11485–11504. doi: 10.5194/acp-12-11485-2012
- Pavelin, E. G., Johnson, C. E., Rughooputh, S., & Toumi, R.** (1999). Evaluation of pre-industrial surface ozone measurements made using scho nbein's metho.

- Atmospheric Environment*, 33, 919–929. doi: 10.1016/S1352-2310(98)00257-X
- Pleijel, H.** (2007). Transboundary air pollution. *Studentlitteratur*.
- Pleim, J. E., & Xiu, A.** (1995). Development and testing of a surface flux and planetary boundary layer model for application in mesoscale models. *Journal of Applied Meteorology*, 34, 16-32.
- Ramankutty, N., Evan, A., Monfreda, C., & Foley, J.** (2008). Farming the planet: 1. geographic distribution of global agricultural lands in the year 2000. *Global Biogeochemical Cycles*, 22(GB1003). doi: 10.1029/2007GB002952
- Reich, P., & Amundson, R.** (1985). Ambient levels of ozone reduce net photosynthesis in tree and crop species. *Science*, 230, 566 - 570.
- Roy, S., Beig, G., & Ghude, D.** (2009). Exposure-plant response of ambient ozone over the tropical indian region. *Atmospheric Chemistry and Physics*, 9(3), 5253-5260.
- Royal Society.** (2008). *Ground-level ozone in the 21st century: future trends, impacts and policy implications* (Tech. Rep.). Retrieved from <http://www.eea.europa.eu/publications/emep-eea-guidebook-2013>
- Sinha, B., & Sangwan, Y. K. V. S. C. C. B. S. V., K. and Maurya.** (2015). Assessment of crop yield losses in punjab and haryana using 2 years of continuous in situ ozone measurements. *Atmospheric Chemistry and Physics*, 15, 9555–9576.
- Skamarock, W. C., Klemp, J. B., Dudhia, J., Gill, D. O., Barker, D. M., Duda, M. G., ... Powers, J. G.** (2008). *A description of the advanced research wrf version 3, national center for atmospheric research technical note, ncar/tn-475+str* (Tech. Rep.). Retrieved from <http://esa.un.org/unpd/wup/Highlights/WUP2014-Highlights.pdf>
- Staehelin, J., Thudium, J., Buehler, R., Volz-Thomas, A., & Graber, W.** (1994). Trends in surface ozone concentrations at arosa (switzerland). *Atmospheric Environment*, 28(1), 75–87.
- Stevenson, D., Young, P. J., Naik, V., Lamarque, D. T., J.-F. and Shindell, Voulgarakis, A., Skeie, R. B., ... Archibald, A.** (2013). Tropospheric ozone changes, radiative forcing and attribution to emissions in the atmospheric chemistry and climate model intercomparison project (accmip). *Atmos. Chem. Phys.*, 13, 3063–3085. doi: 10
- Stroud, C. A., Makar, P. A., Moran, M. D., Gong, S., W. and Gong, Zhang, J., Hayden, K., ... Slowik, J. G.** (2011). Impact of model grid spacing on regional- and urban- scale air quality predictions of organic aerosol. *Atmospheric Chemistry and Physics*, 11, 3107-3118.
- Thouret, V., Cammas, J.-P., Sauvage, B., Athier, G., Zbinden, R., Nedelec, P., ... Karcher, F.** (2006). Tropopause referenced ozone climatology and inter-annual variability (1994–2003) from the mozaic programme. *Atmospheric Chemistry and Physics*, 6, 1033–1051. doi: 10.5194/acp-6-1033-2006
- Tong, D. Q., Mathur, R., Kang, D., Yu, S., Schere, K. L., & G. Pouliot, G.** (2009). Vegetation exposure to ozone over the continental united states: Assessment of exposure indices by the eta-cmaq air quality forecast model. *Atmospheric Environment*, 43(3), 724-733.
- Unal, A., Frey, H. C., & Roupail, N. M.** (2004). Quantification of highway vehicle emissions hot spots based upon on-board measurements. *J. Air Waste Manage.*



- United Nations (UN).** (2016). *Department of economic and social affairs*. Retrieved 21.02.2016, from <http://esa.un.org/unpd/wpp/>
- USEPA.** (1996). *Air quality criteria for ozone and other photochemical oxidants, vol. ii. epa-600/p-93/00bf, us environmental protection agency, national center for environmental assessment, us environmental protection agency, national center for environmental assessment, nc, usa* (Tech. Rep.).
- Van Dingenen, F. R. F. K. M. E. L. C. J., R. and Dentener.** (2009). The global impact of ozone on agricultural crop yields under current and future air quality legislation. *Atmospheric Environment*, 3, 604-618.
- Vingarzan, R.** (2004). A review of surface ozone background levels and trends. *Atmospheric Environment*, 38, 3431-3442.
- Wang, X., & Mauzerall, D.** (2004). Characterizing distribution of surface ozone and its impact on grain production in china, japan and south korea: 1990 and 2020. *Atmospheric Environment*, 38, 4383 – 4402.
- Wilkinson, S., Mills, G., Illidge, R., & Davies, J.** (2011). How is ozone pollution reducing our food supply. *Journal of Experimental Botany*.
- Yardwood, G., Rao, S., Yocke, M., & Whitten, G. Z.** (2005). *Updates to the carbon bond chemical mechanism: Cb05. final report to the us epa, rt-0400675*. (Tech. Rep.). Retrieved from <https://www.cmascenter.org>
- Young, P., Archibald, A. T., Bowman, K. W., Lamarque, J.-F., Naik, V., Stevenson, S., D. S. and Tilmes, ... Zeng, G.** (2013). Pre-industrial to end 21st century projections of tropospheric ozone from the atmospheric chemistry and climate model intercomparison project (accmip). *Atmos. Chem. Phys.*, 13, 2063–2090. doi: 10



## **APPENDICES**

**APPENDIX A:** WRF Model Performance Results

**APPENDIX B:** Lists of Total Crop Production Loss for Each Country

**APPENDIX C:** Lists of Total Economic Loss for Each Country

**APPENDIX D:** CMAQ Model Performance Results



## APPENDIX A

**Table A.1** : Model Performance Analysis for Temperature at 2m for Each Station at the nested domain (10km resl.)

Stations	MB (°C)	NMB (%)	RMSE (°C)	R <sup>2</sup>
Erzurum	-5.01	-0.40	5.87	0.60
Inebolu	-3.91	-0.21	4.89	0.79
Trabzon	-6.78	-0.35	7.75	0.46
Aydın	-4.09	-0.16	4.56	0.89
Mugla	-5.64	-0.24	6.23	0.85
Antalya	-1.80	-0.07	2.96	0.81
Diyarbakir	-2.88	-0.13	4.57	0.79
Konya	-4.20	-0.23	5.15	0.74
Kirklareli	-4.63	-0.20	5.11	0.85

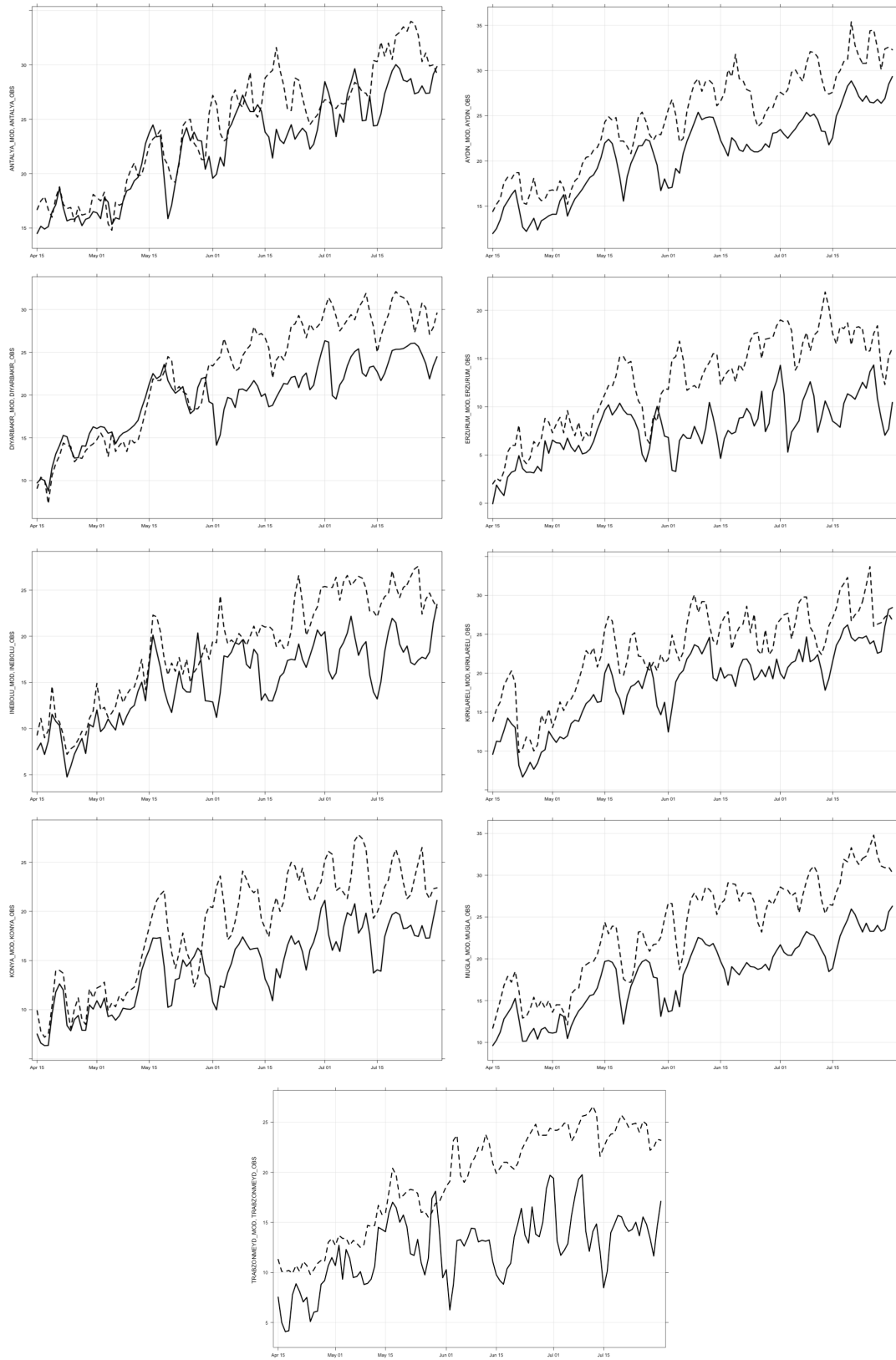


**Figure A.1 :** Modelled (line) and Observed (dash-line) 2-m Temperature (°C ) Time Series for 9 stations:  
 (a) Antalya, (b) Aydın, (c) Diyarbakır, (d) Erzurum, (e) İnebolu, (f) Kırklareli, (g) Konya, (h) Muğla, (i) Trabzon

## APPENDIX B

**Table B.1 : Country-Specific Total Wheat Production and Total Crop Production Loss for three Ozone Exposure Indices**

	Region	Total Wheat Production (FAO 2009 Data, Ton)	AOT40 Based Estimated CPL (Ton)	M7 Based Estimated CPL (Ton)	W126 Based Estimated CPL (Ton)
Russia	Other Countries	61740	7142	17294	721
France	Western Europe	38332	2370	3370	214
Germany	Central Europe	25192	2723	2449	447
Ukraine	Eastern Europe	20887	4134	6648	678
Turkey	Other Countries	20600	3225	6813	472
United Kingdom	Northern Europe	14076	24	119	1
Iran	Other Countries	13484	1020	2281	95
Poland	Central Europe	9790	1320	1236	238
Egypt	Other Countries	8523	3147	5456	422
Italy	Southern Europe	6535	5082	6457	1539
Denmark	Northern Europe	5940	135	195	11
Romania	Eastern Europe	5203	1460	2262	226
Spain	Southern Europe	4805	290	489	26
Hungary	Central Europe	4419	1341	1706	261
Czech Republic	Central Europe	4358	975	900	180
Bulgaria	Eastern Europe	3977	1158	1968	186
Syria	Other Countries	3702	410	1079	37
Sweden	Northern Europe	2278	64	102	5
Lithuania	Northern Europe	2100	98	204	9
Azerbaijan	Other Countries	2096	155	626	15
Serbia	Eastern Europe	2068	545	814	85
Belarus	Northern Europe	1979	235	357	38
Belgium	Western Europe	1910	60	69	4
Greece	Southern Europe	1830	745	1058	152
Iraq	Other Countries	1700	113	340	10
Tunisia	Other Countries	1654	493	537	91
Slovakia	Central Europe	1538	442	484	93
Austria	Central Europe	1523	322	398	50
Netherlands	Western Europe	1402	18	23	1
Latvia	Northern Europe	1036	43	92	4
Croatia	Eastern Europe	936	578	638	176
Finland	Northern Europe	887	31	52	2
Moldova	Eastern Europe	737	159	255	23
Ireland	Northern Europe	690	5	8	0
Switzerland	Central Europe	550	91	129	12
Estonia	Northern Europe	343	12	28	1
Albania	Southern Europe	333	294	319	91
Norway	Northern Europe	278	4	11	0
Macedonia	Eastern Europe	271	58	99	9
Bosnia	Eastern Europe	256	76	98	13
Armenia	Other Countries	198	2	33	0
Israel	Other Countries	133	54	81	6
Portugal	Southern Europe	124	9	8	1
Lebanon	Other Countries	111	17	37	2
Georgia	Other Countries	54	3	13	0
Jordan	Other Countries	12	1	3	0
Montenegro	Eastern Europe	3	1	1	0
Slovenia	Central Europe	1	1	1	0

**Table B.2 : Country-Specific Percentage of Total Crop Production Loss for three Ozone Exposure Indices**

Country Name	Region	AOT40 Based	M7 Based	W126 Based
		Estimated CPL Percent (%)	Estimated CPL Percent (%)	Estimated CPL Percent (%)
Russia	Other Countries	11.57	28.01	1.17
France	Western Europe	6.18	8.79	0.56
Germany	Central Europe	10.81	9.72	1.77
Ukraine	Eastern Europe	19.79	31.83	3.25
Turkey	Other Countries	15.65	33.07	2.29
United Kingdom	Northern Europe	0.17	0.85	0
Iran	Other Countries	7.57	16.92	0.7
Poland	Central Europe	13.49	12.62	2.43
Egypt	Other Countries	36.93	64.02	4.96
Italy	Southern Europe	77.76	98.81	23.55
Denmark	Northern Europe	2.28	3.28	0.19
Romania	Eastern Europe	28.07	43.48	4.34
Spain	Southern Europe	6.04	10.17	0.54
Hungary	Central Europe	30.35	38.61	5.9
Czech Republic	Central Europe	22.36	20.66	4.14
Bulgaria	Eastern Europe	29.12	49.48	4.68
Syria	Other Countries	11.07	29.14	1
Sweden	Northern Europe	2.82	4.47	0.23
Lithuania	Northern Europe	4.65	9.69	0.43
Azerbaijan	Other Countries	7.39	29.86	0.73
Serbia	Eastern Europe	26.36	39.36	4.09
Belarus	Northern Europe	11.89	18.02	1.94
Belgium	Western Europe	3.14	3.6	0.21
Greece	Southern Europe	40.71	57.82	8.29
Iraq	Other Countries	6.65	19.98	0.6
Tunisia	Other Countries	29.81	32.47	5.51
Slovakia	Central Europe	28.76	31.45	6.05
Austria	Central Europe	21.15	26.1	3.26
Netherlands	Western Europe	1.28	1.65	0.06
Latvia	Northern Europe	4.14	8.85	0.34
Croatia	Eastern Europe	61.71	68.16	18.8
Finland	Northern Europe	3.44	5.91	0.28
Moldova	Eastern Europe	21.54	34.64	3.18
Ireland	Northern Europe	0.72	1.2	0.02
Switzerland	Central Europe	16.49	23.46	2.11
Estonia	Northern Europe	3.6	8.03	0.38
Albania	Southern Europe	88.23	95.68	27.39
Norway	Northern Europe	1.49	4.02	0.12
Macedonia	Eastern Europe	21.23	36.70	3.27
Bosnia	Eastern Europe	29.8	38.31	5.09
Armenia	Other Countries	1.16	16.77	0.16
Israel	Other Countries	40.72	61.01	4.45
Portugal	Southern Europe	7.19	6.66	0.62
Lebanon	Other Countries	14.99	33.340	1.41
Georgia	Other Countries	5.9	23.57	0.62
Jordan	Other Countries	9.57	26.16	0.76
Montenegro	Eastern Europe	46.22	49.04	11.47
Slovenia	Central Europe	55.62	59.06	14.83



## APPENDIX C

**Table C.1 : Country-Specific FAO 2009 Producer Price [USD] and Total Economic Loss [USD] for three Ozone Exposure Indices**

ID	Country Name	Region	FAO Producer Price USD/tonne	AOT40 Economic Loss	M7 Economic Loss	W126 Economic Loss
34	Russia	Other Countries	134.72	962203526.80	2329909139	97108336.75
8	France	Western Europe	155.37	368248455.30	523575463.10	33199295.15
9	Germany	Central Europe	156.94	427421208.5	384362569.80	70166349.77
31	Ukraine	Eastern Europe	101.67	420308557.5	675908023.70	68926719.06
35	Turkey	Other Countries	328.39	1058899902	2237248302	155063270.90
22	United Kingdom	Northern Europe	181.25	4333118.5	21628178.79	98599.11
46	Iran	Other Countries	309.61	315927409.10	706256850.79	29269109.16
15	Poland	Central Europe	155.81	205690635.10	192507603	37085198.9
37	Egypt	Other Countries	291.16	916405446.6	1588615941	123004939.5
12	Italy	Southern Europe	253.61	1288746868	1637534723	390282877.10
5	Denmark	Northern Europe	169.35	22916765.26	33040660.67	1892969.11
17	Romania	Eastern Europe	154.61	225764330.80	349775773.70	34884284.63
20	Spain	Southern Europe	222.64	64567817.14	108762290.2	5782430.79
10	Hungary	Central Europe	148.82	199610492.20	253905688.40	38781731.75
4	Czech Republic	Central Europe	144.88	141190805.7	130418684.9	26116092.81
2	Bulgaria	Eastern Europe	150	173685506.9	295160770.4	27920601.9
38	Syria	Other Countries	406.48	166594028.4	438543781	14976649.2
21	Sweden	Northern Europe	149.8	9626260.75	15245320.13	772489.69
13	Lithuania	Northern Europe	161.41	15762607.38	32870918.69	1464201.83
43	Azerbaijan	Other Countries	274.95	42569737.27	172123559.9	4195777.71
26	Serbia	Eastern Europe	145.05	79056240.09	118055554	12277836.27
32	Belarus	Northern Europe	132.93	31270260.29	47415064.73	5096420.5
1	Belgium	Western Europe	153.47	9200229.98	10563086.52	624515.27
23	Greece	Southern Europe	230.21	171518715.1	243597139.7	34933323.36
39	Iraq	Other Countries	512.82	58002988.05	174222780.8	5210147.42
36	Tunisia	Other Countries	318.52	156984690.2	171036798.8	29017619.13
18	Slovakia	Central Europe	159.89	70718742.63	77321948.46	14883708.97
0	Austria	Central Europe	126.39	40716534.73	50246278.25	6286430.79
14	Netherlands	Western Europe	153.56	2763851.94	3557494.56	124618.08
47	Latvia	Northern Europe	160	6866896.59	14681593.23	563511.28
3	Croatia	Eastern Europe	159.2	91959755.79	101568762	28014214.59
7	Finland	Northern Europe	183.33	5601621.73	9604455.78	447516.06
30	Moldova	Eastern Europe	86.5	13725422.62	22071082.15	2025388.61
11	Ireland	Northern Europe	145.83	723977.76	1204969.23	16119.15
24	Switzerland	Central Europe	406.48	36858148.64	52429780.81	4707421.25
6	Estonia	Northern Europe	146.57	1807972.68	4032560.27	190756.26
28	Albania	Southern Europe	273.75	80454288.94	87244889.23	24974020.03
33	Norway	Northern Europe	367.2	1523346.62	4104811.11	121897.83
29	Macedonia	Eastern Europe	159.41	9174500.58	15860135.02	1412744.06
25	Bosnia	Eastern Europe	194.29	14814416.83	19044354.46	2531042.78
44	Armenia	Other Countries	264.55	605976.73	8788129.3	83934.54
41	Israel	Other Countries	303.82	16448586.56	24644274.52	1795904.73
16	Portugal	Southern Europe	316.67	2827954.46	2617594.8	244895.12
40	Lebanon	Other Countries	364.84	6092562.49	13550645.73	574339.79
45	Georgia	Other Countries	232.93	740763.54	2959675.35	77510.84
42	Jordan	Other Countries	418.31	499848.91	1366224.64	39919.04
27	Montenegro	Eastern Europe	156.65	220380.31	233840.42	54692.43
19	Slovenia	Central Europe	165.69	87554.76	92968.96	23342.93

**Table C.2 : Country-Specific Economic Damages in terms of EL/GDP (percentage)**  
(normalized values to make comparison)

Country Name	Region	GDP at market prices (current Million US\$)	AOT40 Based Estimated EL/GDP (%)	M7 Based Estimated EL/GDP (%)	W126 Based Estimated EL/GDP (%)	Wheat Production in GDP (%)
Italy	Southern Europe	2186239.35	5.9E-4	7.49E-4	1.79E-4	7.58E-4
Turkey	Other Countries	614553.92	1.72E-3	3.64E-3	2.52E-4	1.10E-2
Russia	Other Countries	1222644.28	7.87E-4	1.91E-3	7.94E-5	6.8E-3
Egypt	Other Countries	188982.38	4.85E-3	8.41E-3	6.51E-4	1.31E-2
Germany	Central Europe	3418005.0	1.25E-4	1.13E-4	2.05E-5	1.16E-3
Ukraine	Eastern Europe	117227.77	3.59E-3	5.77E-3	5.88E-4	1.81E-2
France	Western Europe	2693827.45	1.37E-4	1.94E-4	1.23E-5	2.21E-3
Iran	Other Countries	398978.10	7.92E-4	1.77E-3	7.34E-5	1.05E-2
Romania	Eastern Europe	167422.95	1.35E-3	2.09E-3	2.08E-4	4.80E-3
Poland	Central Europe	436476.39	4.71E-4	4.41E-4	8.5E-5	3.49E-3
Hungary	Central Europe	129774.04	1.54E-3	1.96E-3	2.99E-4	5.07E-3
Bulgaria	Eastern Europe	51783.45	3.35E-3	5.70E-3	5.39E-4	1.15E-2
Greece	Southern Europe	330000.25	5.2E-4	7.382E-4	1.06E-4	1.28E-3
Tunisia	Other Countries	43454.94	3.61E-3	3.94E-3	6.68E-4	1.21E-2
Czech Republic	Central Europe	205729.79	6.86E-4	6.34E-4	1.27E-4	3.07E-3
Croatia	Eastern Europe	62703.1	1.47E-3	1.62E-3	4.47E-4	2.38E-3
Albania	Southern Europe	12044.21	6.68E-3	7.24E-3	2.07E-3	7.57E-3
Serbia	Eastern Europe	42616.65	1.85E-3	2.77E-3	2.88E-4	7.04E-3
Slovakia	Central Europe	88661.44	7.98E-4	8.72E-4	1.68E-4	2.77E-3
Spain	Southern Europe	1499074.74	4.31E-5	7.26E-5	3.86E-6	7.14E-4
Iraq	Other Countries	111660.85	5.19E-4	1.56E-3	4.66E-5	7.81E-3
Azerbaijan	Other Countries	44291.49	9.61E-4	3.88E-3	9.47E-5	1.30E-2
Austria	Central Europe	397594.27	1.02E-4	1.26E-4	1.58E-5	4.84E-4
Switzerland	Central Europe	539528.23	6.83E-5	9.72E-5	8.73E-6	4.14E-4
Belarus	Northern Europe	49208.65	6.35E-4	9.63E-4	1.04E-4	5.35E-3
Denmark	Northern Europe	319762.35	7.17E-5	1.03E-4	5.92E-6	3.15E-3
Israel	Other Countries	208068.81	7.91E-5	1.18E-4	8.63E-6	1.94E-4
Lithuania	Northern Europe	37440.67	4.21E-4	8.78E-4	3.91E-5	9.05E-3
Bosnia	Eastern Europe	17600.63	8.42E-4	1.08E-3	1.44E-4	2.82E-3
Moldova	Eastern Europe	5439.42	2.52E-3	4.06E-3	3.72E-4	1.17E-2
Sweden	Northern Europe	429657.03	2.24E-5	3.55E-5	1.79E-6	7.94E-4
Belgium	Western Europe	484552.65	1.90E-5	2.18E-5	1.29E-6	6.05E-4
Macedonia	Eastern Europe	9401.73	9.76E-4	1.69E-3	1.50E-4	4.59E-3
Latvia	Northern Europe	26144.61	2.63E-4	5.62E-4	2.16E-5	6.34E-3
Lebanon	Other Countries	35139.64	1.73E-4	3.86E-4	1.63E-5	1.16E-3
Finland	Northern Europe	251499.03	2.23E-5	3.82E-5	1.78E-6	6.47E-4
United Kingdom	Northern Europe	2314577.04	1.87E-6	9.34E-6	4.26E-8	1.10E-3
Portugal	Southern Europe	243745.75	1.16E-5	1.07E-5	1.0E-6	1.61E-4
Netherlands	Western Europe	857932.76	3.22E-6	4.15E-6	1.45E-7	2.51E-4
Estonia	Northern Europe	19652.49	9.2E-5	2.05E-4	9.71E-6	2.55E-3
Norway	Northern Europe	386383.92	3.94E-6	1.06E-5	3.15E-7	2.64E-4
Georgia	Other Countries	10766.84	6.88E-5	2.75E-4	7.2E-6	1.17E-3
Ireland	Northern Europe	235387.17	3.08E-6	5.12E-6	6.85E-8	4.27E-4
Armenia	Other Countries	8647.94	7.01E-5	1.01E-3	9.71E-6	6.06E-3
Jordan	Other Countries	23818.32	2.1E-5	5.74E-5	1.67E-6	2.19E-4
Montenegro	Eastern Europe	4141.38	5.32E-5	5.65E-5	1.32E-5	1.15E-4
Slovenia	Central Europe	50244.79	1.74E-6	1.85E-6	4.65E-7	3.13E-6

## APPENDIX D

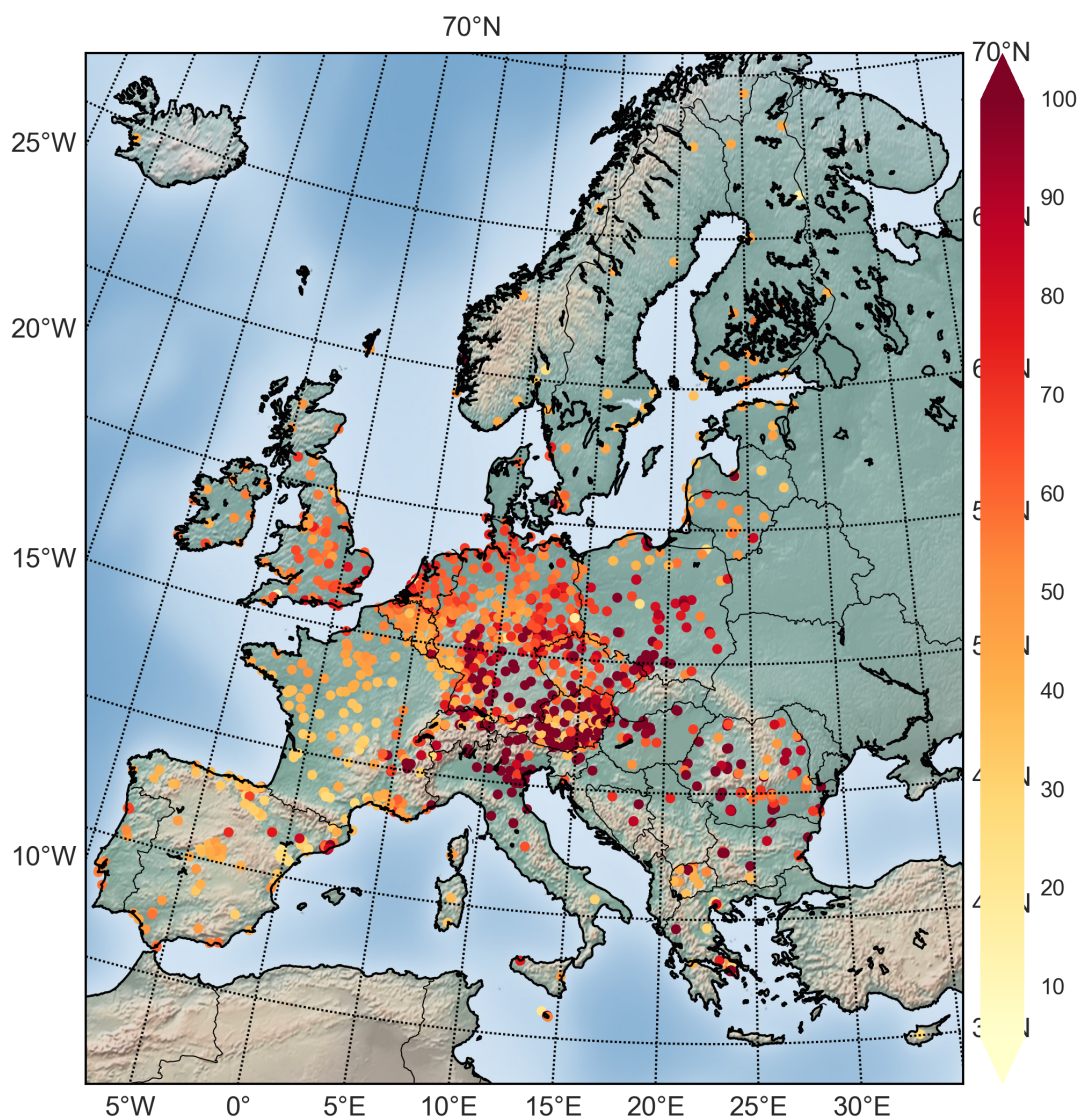


**Figure D.1** : Mean Normalized Error (MNE) Results (%) for Each Station in the Airbase

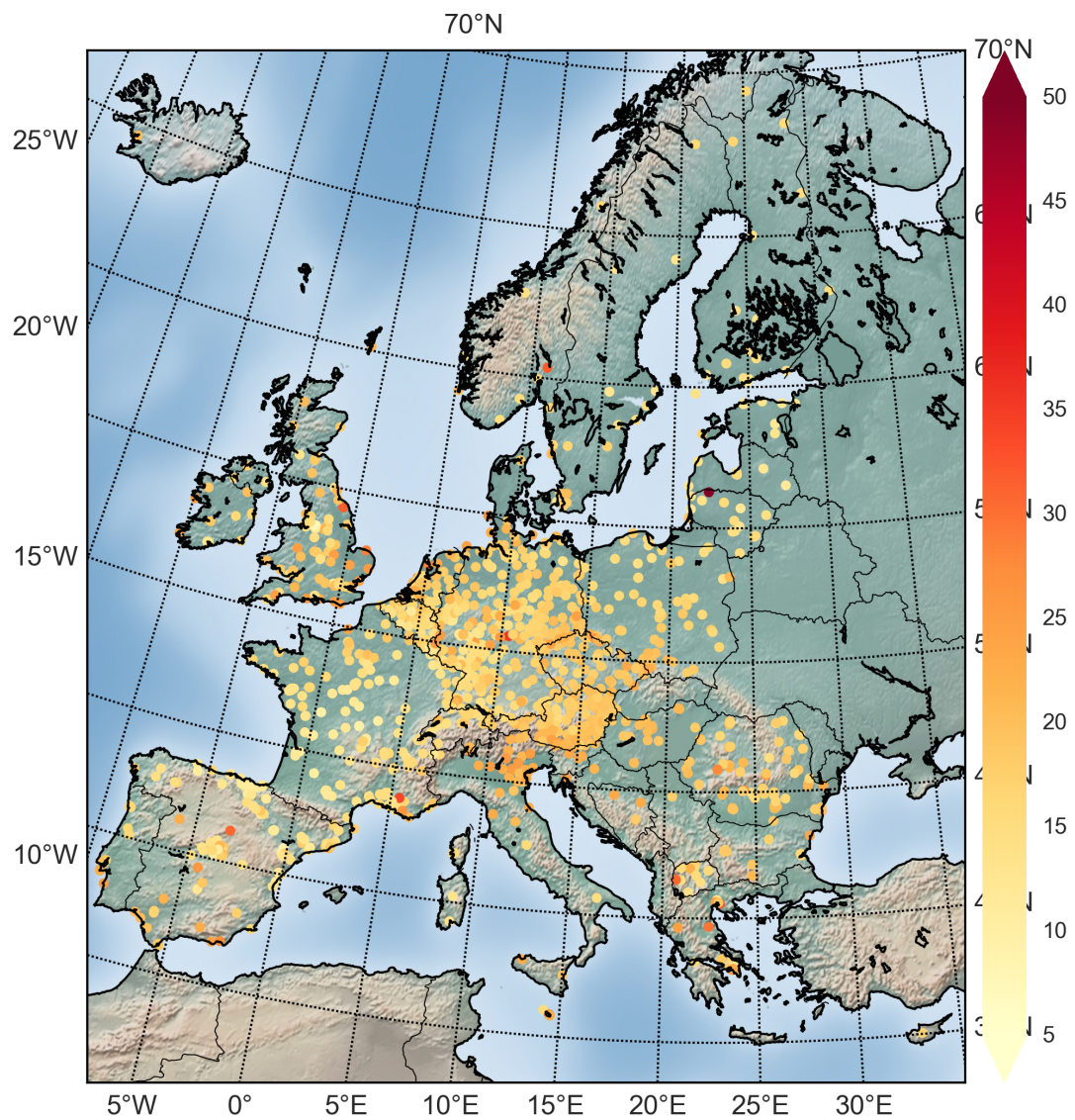


**Figure D.2 :** Root Mean Square Error (RMSE) Results (ppb) for Each Station in the Airbase

## CURRICULUM VITAE



**Name Surname:** YAŞAR BURAK ÖZTANER

**Place and Date of Birth:** Diyarbakır, 08/01/1990

**E-Mail:** oztaner@itu.edu.tr, burakoztaner@gmail.com

**B.Sc.:** 2008-2013 Department of Meteorological Engineering, Istanbul Technical University

### Professional Experience and Rewards:

5th Air Pollution and Control Symposium (HKK2013), Eskisehir, Turkey - TUBITAK Young Scientist Travel Award - 2013

15th EMS Annual Meeting 12th European Conference on Application of Meteorology (ECAM), Sofia - Bulgaria -EMS Young Scientist Travel Award (YSTA) - 2015

Visiting Scholar, Department of Civil and Environmental Engineering, Carleton University, Ottawa, Ontario, Canada (September, 2014 – March 2015)

16th EMS Annual Meeting 11th European Conference on Application of Climatology (ECAC), EMS and Tromp Foundation Young Scientist Travel Award (YSTA)- 2016

### List of Publications and Patents:

**Oztaner, Y.B.**, Kahraman, A., Çalışkan, E., Tanrıöver Ş.T., Kahya, C., Aksoy, B., İncecik, S., Topçu, S., Arslan, Z., Barutçu, B., Sezen, İ., SAKarya, S., Deniz : A. Evaluation Of The Aerosol Impact On The Short Term Prediction Of Global Solar Radiation Using WRF Model At Clear Sky Condition. Hava Kirliliği Araştırmaları Dergisi. 07/2014; 3(1):2-11. (Turkish)(Peer-Reviewed)

**Oztaner, Y.B.**, Kahya, C., Bektas Balcik, F., Ozcomak, D., Seker, Z.D. : Spatio-Temporal Analysis Of Pm2.5 over Marmara Region, Turkey.(Submitted, peer-reviewed Int.Jour.Fresenius Environmental Bulletin (FEB))

Kahya, C., Balcik, F.B., **Oztaner, Y.B.**, Guney, B. : Determining Land Surface Temperature Relations with Land Use-Land Cover and Air Pollution. General Assembly 2016, European Geoscience Union (EGU), April 2016. (Oral Presentation)

**Oztaner, Y.B.**, Pappin, A., Zhao, S., Pozzoli, L., Hakami, A., Kindap, T., Unal, A.: Determination of Crop Yield Loss due to Ozone Damage via CMAQ Adjoint over Europe. 14th Annual CMAS Conference, Chapel Hill, NC, USA; October 2015. (Poster Presentation)



**Oztaner, Y.B.**, Pozzoli, L., Hakami, A., Kindap, T., Unal, A.: Impact of Land-Use Types and Urban Canopy Structure on Urban Heat Island via High Resolution WRF Modeling: Istanbul Case Study. 15th EMS Annual Meeting 12th European Conference on Application of Meteorology (ECAM), Sofia, Bulgaria; Sep. 2015. (Oral Presentation)

Ozcomak, D., **Oztaner, Y.B.**, Pozzoli, L., Kindap, T., Unal, A.: A Statistical Comparison of Observed and Modelled Daily PM10 Levels in Marmara Region. 15th EMS Annual Meeting 12th European Conference on Application of Meteorology (ECAM), Sofia, Bulgaria; Sep. 2015. (Oral Presentation)

**Oztaner, Y.B.**, Guney, B., Ozcomak, D., Kalkan, K., Balçık, F.B., Kahya, C., Çakır, S. : Spatio-Temporal Analysis of PM2.5 over Marmara Region, Turkey. 18th International Symposium on Environmental Pollution and Its Impact on Life in the Mediterranean Region (MESAEP), Crete, Greece; Sep. 2015. (Oral Presentation)

**Oztaner, Y.B.**, Kahya, C., Incecik S. : The Impact of Aerosols on Global Horizontal Irradiance over Southeastern Anatolia of Turkey. 34th International Technical Meeting on Air Pollution Modeling and its Applications (ITM), May 2015, Montpellier, France (In press)

**Oztaner, Y.B.**, Pozzoli, L., Hakami, A., Kindap, T., Unal, A. : Investigation of the Impact of Land Use Modification to the Urban Heat Island Phenomena Using WRF over Istanbul. 7th Atmospheric Science Symposium (ATMOS2015), Istanbul, Turkey; April 2015. (Oral Presentation)

**Oztaner, Y.B.**, Guney, B., Ozcomak, D., Kalkan, K., Balçık, F.B., Kahya, C., Çakır, S. : An Investigation of the the Relationship between MODIS AOD and PM2.5 over Marmara Region, Turkey . 7th Atmospheric Science Symposium (ATMOS2015), Istanbul, Turkey; April 2015. (Oral Presentation)

Ergul, M.G., **Oztaner, Y.B.**, Unal, A., Kindap, T. : Comparative Analysis of Fog Prediction Algorithms via Use of WRF Model over Istanbul. 14th EMS Annual Meeting 10th European Conference on Applied Climatology (ECAC), Prague, Czech Republic; October 2014 (Oral presentation)

**Oztaner, Y.B.**, Guney, B., Kahya, C.:Trend Analysis in the MODIS Aerosol Optical Depth over Turkey. 14th EMS Annual Meeting 10th European Conference on Applied Climatology (ECAC), Prague, Czech Republic; October 2014. (Poster presentation)

**Oztaner, Y.B.**, Guney, B., Kalkan, K., Kahya, C., Balçık, F.B., Çakır, S. : Comparison of Interpolation Techniques to Determine PM2.5 Distribution: Marmara Region Case Study. (Turkish). 5th Remote Sensing and GIS Symposium (UZAL-CBS2014), Istanbul-Turkey; October 2014. (Poster presentation)

**Oztaner, Y.B.**, Kahya, C., Incecik, S. : The Impact of Aerosols on Global Horizontal Irradiance over Southeastern Anatolia of Turkey. 5th European Chemistry Congress (EuCheMS), WOW Istanbul Convention Center, Istanbul, Turkey; September 2014. (Oral presentation)

**Oztaner, Y.B.**, Kahya, C., Incecik, S. : The Impact of Aerosols on Global Horizontal Irradiance over Southeastern Anatolia of Turkey. 13th European Meteorological Society (EMS) Annual Meeting and 11th ECAM, Reading-England; September 2013. (Poster presentation)

**Oztaner, Y.B.**, Ozdemir, E.T., Sezen, I., Deniz, A., Efe, B. : An Examination Of Atmospheric Transports Of Sand And Dust And Pm10 Profiles At Airports Over Turkey On 18 April 2012 When Southern Storm Has Been Occurred. OSTIV 2013, Meteorological Panel, Antalya-Turkey September 2013. (Oral presentation)

**Oztaner, Y.B.**, Kahraman,A., Caliskan, E.,Tanriover, S.T., Kahya, C., Aksoy, B., Incecik, S., Topcu, S.,Arslan, Z., Barutcu, B:, Sezen, I., Sakarya, S., Deniz, A. : Evaluation of the Aerosol Effect on Short Term Forecasting of Global Solar Radiation using WRF Model. (Turkish) 5th Air Pollution and Controlling Symposium, Eskisehir; September 2013. (Oral presentation)

Ozcomak, D., **Oztaner, Y.B.**, Ozturk, A:, Toros, H., Deniz, A.: Investigation of BTEX Measurements with Meteorological Parameters in Istanbul.(Turkish) 5th Air Pollution and Controlling Symposium, Eskisehir; September 2013. (Oral presentation)

Ozcomak, D., **Oztaner, Y.B.**, Ozturk, A:, Toros, H. : Investigation of O-Xylene and Styrene Concentrations for Kagithane Air Quality Station, Istanbul. 6th Atmospheric Science Symposium - ATMOS 2013, Istanbul; April 2013. (Poster presentation)

**Oztaner, Y.B.**, Yilmaz, A : An Examination of Fog and PM10 Relationship for Ataturk and Esenboga International Airports of Turkey. 6th Atmospheric Science Symposium - ATMOS 2013, Istanbul; April 2013. (Oral presentation)

**Oztaner, Y.B.**, Sakarya, S. : Evaluation of Three Interpolation Methods for Particulate Matter Pollution Distribution under The Influence of Inversion as a Case Study for Istanbul and Izmit. Air Quality Management at Urban, Regional And Global Scales 4th International Symposium and IUAPPA Regional Conference, Istanbul; September 2012. (Oral presentation)